mitte etwas bei. Man wird also erwarten, daß die Flügel der aus Achsennähe emittierten Linien durch die Randzonen unbeeinflußt bleiben.

Wendet man an Stelle der Halbwertsbreite eine Vergleichsgröße an, die mehr im Linienflügel liegt – z. B. den Wellenlängenabstand $(Z-H)$ zwischen den beiden Punkten, zwischen welchen die Intensität von 1/2 auf 1/10 der Maximalintensität abgenommen hat –, so kann man erwarten, daß die Elektronendichte unter der gemachten Voraussetzung auch ohne ABEL-Inversion in guter Näherung gefunden werden kann.

Die in Abb. 3 dargestellten Elektronendichteprofile wurden auf die beschriebene Weise mit Hilfe der Vergleichsgröße $(Z-H)$ ermittelt. Die Genauigkeit des Verfahrens wurde für den Bogen (a) überprüft. Dazu wurde das gemessene Temperatur- und Elektronendichteprofil des Bogens durch je ein Treppenprofil mit fünf Stufen ersetzt. Für jede Stufe wurde nach [7] die Kontur der H_γ-Linie berechnet. Aus der Überlagerung der Strahlung der verschiedenen Zonen erhält man die entsprechenden „side-on"-Profile der Linie. Ein Vergleich mit den Ausgangsprofilen zeigte, daß die unter Verwendung von $(Z-H)$ bestimmte Elektronendichte in der Bogenmitte um etwa 20% zu klein ist. (Der aus der Halbwertsbreite erhaltene Wert dagegen hätte einen Fehler von 40%.) Dies wirkt sich bei der Temperaturbestimmung nach Verfahren b) so aus, daß die Temperaturwerte in der Bogenachse zu klein ausfallen; am Rande dagegen ist die Methode genau.

Spallation, Fission, and Neutron Capture Anomalies in Meteoritic Krypton and Xenon

K. MARTI *, P. EBERHARDT, and J. GEISS

Physikalisches Institut, University of Berne, Switzerland

(Z. Naturforschg. **21 a**, 398—413 [1966]; received 19 November 1965)

Measurements of the Kr and Xe concentrations and isotopic compositions in five meteorites are reported. Experimental techniques and reproducibility are discussed in detail. In the Stannern achondrite 75% of the total Kr and 30% of the total Xe are due to cosmic ray induced spallation reactions. Also Bruderheim and H-Ausson show distinct spallation components. The isotopic composition of pure spallation Kr is derived as

$$Kr^{78} : Kr^{80} : Kr^{82} : Kr^{83} : Kr^{84} = 0.179 : 0.495 : 0.765 : 1.00 : 0.63$$

and of spallation Xe as

$$Xe^{124} : Xe^{126} : Xe^{128} : Xe^{130} : Xe^{131} : Xe^{132} = 0.590 : 1.00 : 1.45 : 0.97 : 3.9 : 0.9\,.$$

It is shown that the spallation components found were produced by the cosmic radiation late in the history of the meteorite during a period given by the radiation age. The observed Xe^{126}/Xe^{124} spallation ratio rules out a substantial contribution of spallation products in the xenon of carbonaceous chondrites. The Xe fission spectrum derived by ROWE and KURODA from Pasamonte is corrected for spallation and the following composition is obtained for fission Xe:

$$Xe^{131} : Xe^{132} : Xe^{134} : Xe^{136} = 0.22 : 1.00 : 1.02 : 1.00\,.$$

In Mezö-Madaras and Abee Kr^{80}, Kr^{82} and Xe^{128} excesses are found, due to (n,γ) reactions on Br and I. It is shown that neutrons produced by the cosmic radiation during the radiation age can account for the observed effect in Abee and the evidence so far suggests that this is also true for Mezö-Madaras.

1. Introduction

The concentrations and isotopic composition of xenon in meteorites have been investigated with considerable detail by REYNOLDS and his coworkers [1–5] and others [6, 7]. Meteoritic xenon is a mixture of components which can originate from many different sources, such as the decay of I^{129}, fission of uranium and possibly of transuranium elements, cosmic ray induced spallation reactions and (n,γ)

* Present address: Department of Chemistry, University of California, La Jolla, Calif., U.S.A.

[1] J. H. REYNOLDS, Phys. Rev. Letters **4**, 351 [1960].
[2] D. KRUMMENACHER, C. M. MERRIHUE, R. O. PEPIN, and J. H. REYNOLDS, Geochim. Cosmochim. Acta **26**, 231 [1962].
[3] J. H. REYNOLDS, J. Geophys. Res. **68**, 2939 [1963].
[4] C. M. MERRIHUE, J. Geophys. Res. **68**, 325 [1963].
[5] R. O. PEPIN, in The Origin and Evolution of Atmospheres and Oceans (P. J. BRANCAZIO and A. G. W. CAMERON ed.), J. Wiley and Sons, New York 1964, p. 191.
[6] W. B. CLARKE and H. G. THODE, in Isotopic and Cosmic Chemistry, dedicated to H. C. UREY (H. CRAIG, S. L. MILLER, and G. J. WASSERBURG ed.), North Holland Publ. Co., Amsterdam 1964, p. 471.
[7] M. W. ROWE and P. K. KURODA, J. Geophys. Res. **70**, 709 [1965].

reactions. In addition, varying amounts of trapped xenon (primordial xenon) have been found in all investigated meteorites. Sophisticated experimental techniques have to be applied to disentangle these different components [3]. Results of xenon measurements allow important conclusions to be drawn, concerning the history and conditions prevailing during the formation of meteorites and the solar system. Some of these conclusions, such as the proposed particle irradiation during the early history of the solar system, are, however, based on rather marginal evidence.

The isotopic composition of meteoritic krypton has been investigated less extensively. Anomalies due to spallation reactions and neutron capture in bromine and selenium were reported by CLARKE and THODE [8].

In this paper we report and discuss krypton and xenon measurements on five stone meteorites. One of our main objectives was to investigate the spallation components of meteoritic krypton and xenon and to measure their production rates. In order to enhance the spallation component as opposed to the contribution from other sources, we have selected two meteorites with high but different radiation ages and low trapped gas contents (H-Ausson, Bruderheim) and one meteorite with high Sr, Ba and rare earth concentrations (Stannern). If the spallation component in these meteorites was produced by the cosmic radiation late in the history of the meteorite, it should be proportional to the radiation age and to the concentrations of the target elements (Sr, Zr, Ba, and rare earth elements). For comparison, two meteorites with high trapped gas content (Abee and Mezö-Madaras) were chosen.

2. Meteorite Samples

The sources of our meteorite samples are listed in Table 1, along with other relevant data. The chondrite specimen designated as H-Ausson was sold to us as belonging to the observed fall Ausson. However, we have shown that our specimen is probably mislabeled [13] and have consequently designated it as H-Ausson.

Aliquots of the crushed samples from our helium, neon and argon determinations [13] were available for Bruderheim, H-Ausson and Mezö-Madaras. Stannern was prepared according to the technique described elsewhere [13]. The Abee sample which we received was already powdered. Samples between 100mg and 2.5 g were used, depending on the rare gas content.

3. Experimental Technique

3.1 Rare Gas Extraction and Concentration Determinations

Two different rare gas extraction systems were used: System I was connected directly to the mass spectrometer. The sample was melted in an alundum crucible with a molybdenum insert. The crucible was heated by an internal tungsten heater. Two radiation shields were used. The metal vacuum jacket was water cooled. The meteorite samples, wrapped in Al-foil, were stored in a glass side tube and could be dropped through a fun-

meteorite	sample number	date of fall	recovered weight kg	classification	K-Ar age m.y.	radiation age m.y.	source of sample
Abee*	BE-263	6.10.1952	107	enstatite chondrite	4700	6	b
Bruderheim	BE-70	3.4.1960	300	hypersthene chondrite	1900	26	c
H-Ausson	BE-53	unknown	—	bronzite chondrite	4400	50	d
Mezö-Madaras	BE-175	9.4.1852	23	hypersthene chondrite	2000	26	a
Stannern	BE-234	5.22.1808	52	eucrite	3700	~30**	a

Table 1. Some relevant data on the investigated meteorites. Data from PRIOR and HEY [9]; KEIL [10]; STAUFFER [11]; KIRSTEN, KRANKOWSKY, and ZÄHRINGER [12]; EBERHARDT, EUGSTER, GEISS, and MARTI [13]. — Sources of samples: [a] Prof. W. SCHOLLER, Naturhistorisches Museum, Wien; [b] Dr. F. BEGEMANN, Max-Planck-Institut, Mainz; [c] Prof. R. E. FOLINSBEE, University of Alberta Edmonton; [d] Deyrolle, Paris. * Sample from center of meteorite. ** The radiation age of Stannern was estimated from the Ar^{38} and Ne^{21} concentrations because some He^3 diffusion loss may have occurred in this meteorite [11].

[8] W. B. CLARKE and H. G. THODE, J. Geophys. Res. **69**, 3673 [1964].
[9] G. T. PRIOR and M. H. HEY, Catalogue of Meteorites, British Museum, London 1953.
[10] K. KEIL, Fortschr. Mineral. **38**, 202 [1960].
[11] H. STAUFFER, J. Geophys. Res. **67**, 2023 [1962].
[12] T. KIRSTEN, D. KRANKOWSKY, and J. ZÄHRINGER, Geochim. Cosmochim. Acta **27**, 13 [1963].
[13] P. EBERHARDT, O. EUGSTER, J. GEISS, and K. MARTI, Z. Naturforschg. **21 a**, 414 [1966].

nel into the crucible. The extracted gases were cleaned with a Ti-Zr-sponge getter, a hot CuO – Pd mixture, hot Ti-foil and a hot tungsten ribbon. System II is our standard rare gas extraction system used for the determination of the light rare gases as described by EBERHARDT, EUGSTER, GEISS, and MARTI [13].

Both systems were free of mercury and had no cold traps. Prior to the extraction they were thoroughly baked at 300 °C and the extraction crucible degassed. The samples were heated to 70 °C in order to release adsorbed atmospheric gases. During the extraction the entire systems were kept at approximately 70 °C to avoid adsorption of krypton and xenon. Re-extractions at an increased crucible temperature showed that for both systems the extraction yield was better than 98%.

Prior to the mass spectrometric analyses Xe, Kr, and Ar were separated from He and Ne and from each other by adsorption on charcoal. This was necessary to avoid excessive memory due to high ion currents in the mass spectrometer and to exclude interference on mass 80 from Ar^{40}. Xenon was adsorbed at −78 °C (dry ice-ethanol mixture), Kr at −120 °C (melting point of dry ice-ethanol mixture) and Ar at liquid air temperature. The xenon fraction always contained more than 60% of the Xe; the krypton fraction contained approximately 50% of the Kr and $\lesssim$ 1% of the Ar. No isotopic fractionations due to the separation procedure were detected.

Extraction blanks of both systems were frequently determined from extractions on empty Al-containers and from re-extractions. The blank of system I was 15×10^{-12} cc STP Kr and 3×10^{-12} cc STP Xe; of system II 4×10^{-12} cc STP Kr and 2×10^{-12} cc STP Xe. Extraction system II was also superior in regard to residual organic impurities and had a much lower failure rate. Thus, for most results reported in this paper extraction system II was used.

At least two aliquots of the same sample were extracted to determine the isotopic composition and the reproducibility for each meteorite. The sample size was varied by at least a factor of 2 between these two determinations. Table 2 gives a comparison of the krypton and xenon isotopic compositions obtained in the two analyses of the Stannern achondrite. The agreement is very good, in spite of the low rare gas concentrations and the large anomalies. Also the duplicate analyses of the other meteorites always agreed within the errors given in Tables 4 and 5.

The absolute concentration of xenon was determined in additional extractions using the isotopic dilution method. In order to avoid memory effects, no Xe^{128} spike from irradiated iodine was used. For Abee, which has a large Xe^{129} anomaly, atmospheric xenon was added as spike. The xenon of Abee was used as spike for the other four meteorites by adding small, known amounts of Abee to the meteorite sample. Table 3 gives the results of duplicated isotopic dilution determinations of xenon.

meteorite	sample weight mg	spike	$Xe^{132} \times 10^{-12}$ ccSTP/gm
Abee	150	air xenon standard I	618
Abee	360	air xenon standard II	608
Mezö-Madaras	130	Abee (86 mg)	2050
Mezö-Madaras*	100	air xenon standard I	2200*
Stannern	500	Abee (30 mg)	25.1
Stannern	730	Abee (40 mg)	25.0

Table 3. Reproducibility of xenon concentration measurements with isotopic dilution. * This determination has an error of 10% because the Xe^{129} anomaly in Mezö-Madaras is only 25%.

The krypton concentrations were determined from Kr ion beam intensities in the argon, krypton and xenon fractions. Furthermore, the Kr/Xe ratio (corrected for the different mass spectrometer sensitivity for Kr and Xe) was measured in the unseparated Ar-Kr-Xe fraction of an additional extraction. Kr concentrations were then calculated from the known Xe concentrations. In addition an isotopic dilution determination for Stannern was carried out with Abee as spike. These different modes of the determination of the Kr concentrations always agreed within the limits of error given in Table 4.

sample weight gm	Kr^{78}	Kr^{80}	Kr^{82}	Kr^{83}	Kr^{84}	Kr^{86}			
2.45	70.0	199	341	431	482	100			
0.78	70.5	200	340	427	485	100			
sample weight gm	Xe^{124}	Xe^{126}	Xe^{128}	Xe^{129}	Xe^{130}	Xe^{131}	Xe^{132}	Xe^{134}	Xe^{136}
2.45	7.6	12.7	23.8	98.8	23.0	108.9	100	45.0	40.4
0.78	7.6	12.7	23.6	95.6	23.1	108.5	100	45.1	40.5

Table 2. Comparison of the krypton and xenon isotopic compositions of the two analyses of the Stannern achondrite.

3.2 Mass Spectrometry

The rare gas samples were analyzed in a new, all-glass, sector type, 60 degree, 10 cm radius of curvature, UHV mass spectrometer. The ion current could be measured either with a FARADAY collector or with an electron multiplier. Switchover from one collector to the other could be made in a few seconds. With a source magnet and a total electron emission of 1 mA, the sensitivity of the spectrometer is 0.6×10^{-4} ions/atom sec for krypton and 0.8×10^{-4} ions/atom sec for xenon. This sensitivity corresponds to a detection limit of 2×10^{-15} cc STP per isotope. The mass discrimination was determined by measuring atmospheric krypton and xenon. NIER's [14] values for their isotopic composition were used. All results are corrected for mass discrimination, which was always less than 0.4% per mass unit.

The total amounts of krypton and xenon admitted to the mass spectrometer, including standards, were always kept below a few 10^{-9} cc STP and the instrument was baked frequently at 320 °C, to keep the mass spectrometer memory as low as possible. Also, bombardment with argon ions helped in reducing memory. All isotopic ratios and ion beam intensities were measured as a function of time and all the data were extrapolated to the time of sample introduction.

Even after prolonged baking some background peaks were present at masses 76, 77 and 78, probably due to the C_6H_6 ring. A small correction, deduced from the observed 76 and 77 background, had therefore to be applied to Kr^{78}. However, this correction was always smaller than 3% and the uncertainty of the correction has been included in the error assigned to Kr^{78}. No other hydrocarbon background in the krypton and xenon mass region was present.

A broad background peak at mass 80 was observed when large amounts of Ar were introduced into the mass spectrometer. This background peak could either be due to Ar_2^+ molecules or to charge exchange ($Ar^{++} \rightarrow Ar^+$) between ion source and magnetic analyzer. At argon pressures below 10^{-7} mm Hg the mass 80 peak always disappeared, if the electron energy was reduced below the Ar^{++} appearance potential (44 V). At higher argon pressures ($> 10^{-6}$ mm Hg) the peak at mass 80 could not be eliminated by lowering the electron energy. Thus, at lower pressures only charge exchange contributes to the mass 80 peak, whereas at higher pressures also Ar_2^+ molecules are formed. However, the argon present in the Kr fraction was small enough that no corrections had to be applied. ArKr molecules could interfere with the xenon masses 124 and 126. Therefore, masses 122 and 123 were always monitored during the xenon measurements. These molecules were never observed.

4. Results

The results of our krypton and xenon measurements are given in Tables 4 and 5. For comparison the isotopic composition of atmospheric krypton

meteorite	Kr^{tot}	Kr^{86}	Kr^{78}	Kr^{80}	Kr^{82}	Kr^{83}	Kr^{84}	Kr^{86}
	10^{-12} cc STP/gm							
Abee	2550 ± 300	440	2.03 ± 0.06	17.9 ± 0.2	68.0 ± 0.6	65.7 ± 0.5	326 ± 2	100
Bruderheim	290 ± 50	47	4.28 ± 0.12	20.8 ± 0.2	76.5 ± 0.6	80.1 ± 0.6	335 ± 2	100
H-Ausson	380 ± 80	61	4.76 ± 0.16	21.8 ± 0.4	78.3 ± 0.8	82.0 ± 0.8	337 ± 3	100
Mezö-Madaras	5300 ± 800	913	2.03 ± 0.10	17.7 ± 0.4	68.1 ± 0.8	65.8 ± 0.7	327 ± 2	100
Stannern	170 ± 20	10.5	70.0 ± 0.8	199 ± 3	341 ± 5	431 ± 5	482 ± 4	100
terrestrial atmos.	—	—	2.04	13.1	66.6	66.5	327.6	100

Table 4. Concentrations and isotopic compositions of krypton in the investigated meteorites. The isotopic compositions are normalized to $Kr^{86} \equiv 100\%$. The data for terrestrial krypton are from NIER [14].

meteorite	Xe^{tot}	Xe^{132}	Xe^{124}	Xe^{126}	Xe^{128}	Xe^{129}	Xe^{130}	Xe^{131}	Xe^{132}	Xe^{134}	Xe^{136}
	10^{-12}ccSTP/gm										
Abee	4900	612	0.47	0.42	8.52	524	15.7	81.5	100	38.2	32.2
	± 250		± 0.02	± 0.02	± 0.08	± 15	± 0.1	± 0.5		± 0.2	± 0.2
Bruderheim	400	99	0.56	0.59	8.29	125.2	15.8	81.8	100	38.6	32.5
	± 35		± 0.02	± 0.02	± 0.08	± 1.0	± 0.1	± 0.5		± 0.2	± 0.2
H-Ausson	490	120	0.59	0.65	8.40	129.4	15.8	81.9	100	38.4	32.4
	± 70		± 0.02	± 0.02	± 0.10	± 2.0	± 0.1	± 0.5		± 0.2	± 0.2
Mezö-Madaras	8200	2050	0.46	0.42	8.40	124.1	15.9	81.4	100	38.0	32.0
	± 600		± 0.02	± 0.02	± 0.12	± 1.0	± 0.2	± 0.5		± 0.3	± 0.3
Stannern	115	25	7.6	12.7	23.8	98.0	23.0	108.9	100	45.0	40.4
	± 7		±0.2	± 0.2	± 0.2	± 2.0	± 0.2	± 0.7		± 0.4	± 0.4
terrestrial atmos.	—	—	0.36	0.33	7.14	98.3	15.2	78.8	100	38.8	33.0

Table 5. Concentrations and isotopic compositions of xenon in the investigated meteorites. The isotopic compositions are normalized to $Xe^{132} \equiv 100\%$. The data for terrestrial xenon are from NIER [14].

[14] A. O. NIER, Phys. Rev. **79**, 450 [1950].

meteorite	S %	Cl ppm	Ca %	Fe %	Se ppm	Br ppm	Rb ppm	Sr ppm	Y ppm	Zr ppm	Te ppm	I ppb	Ba ppm	REE ppm	U ppb
Abee	—	530[q]	1.1[a]	32.6[a]	(15)[p]	3.5[l]	—	—	1.0[m]	14[k]	2.2[b]	145[b]	1.8[e]	1.71[m]	11[c]
Bruderheim	2.4[d]	100[q]	1.3[d]	21.9[e]	—	0.3[f,l]*	—	11.2[e]	—	—	0.4[b]	15[b]*	3.4[e]	—	15[b]
H-Ausson	—	—	—	—	—	—	—	—	—	—	—	—	—	—	—
Mezö-Madaras	2.3[g]	—	1.2[g]	24.1[g]	—	—	—	—	—	—	—	—	—	—	—
Stannern	0.31	—	6.8[e]	17.5[e]	—	—	—	85[e]	28[h]	70[k]	—	—	42.2[e]	51.3[h]	—
Average hypersthene chondrites	2.22[n]	110[q]	1.36[n]	21.6[n]	9[p]	0.4[f,l]*	2.8°	11°	2.0[h,m]	11[k]	0.5[b]	35[b]*	3.4[e]	3.4[h,m]	14[c]
Average bronzite chondrites	1.93[n]	100[q]	1.27[n]	27.8[n]	9[p]	0.2[f,l]*	2.8°	11°	2.1[m]	8[k]	0.5[b]	35[b]*	3.4[e]	3.4[h,m]	14[c]

Table 6. Chemical abundances of some elements relevant to the discussion of the krypton and xenon abundance pattern. * Large variations reported.

a Kirsten, Krankowsky, and Zähringer [12]
b Goles and Anders [15]
c Reed, Kigoshi, and Turkevich [16]
d Duke, Maynes, and Brown [17]
e Wyttenbach and Dulakas [18]
f Wyttenbach, von Gunten, and Scherle [19]
g Rammelsberg [20]
h Schmitt, Smith, and Olehy [21]
i Reed [22]
k Schmitt, Bingham, and Chodos [23]
l Merrill [24]
m Schmitt, Smith, Lasch, Mosen, Olehy, and Vasilevskis [25]
n Mason [26]
o Gast [27]
p DuFresne [28]
q von Gunten, Wyttenbach, and Scherle [29]

and xenon is listed. The errors assigned to the individual values are based on the agreement obtained between the duplicate analyses of the particular meteorite. Additional factors, such as sample size, absolute rare gas concentration, uncertainty in extraction blank and correction of mass discrimination were also taken into account. The errors in our gas standards are included in the indicated concentration errors.

In Table 6 chemical abundances of some elements relevant to the discussion of the krypton and xenon results are compiled. The determinations of Wyttenbach and Dulakas [18] were made on aliquots of the samples used for the rare gas measurements.

In Table 7 our results on Bruderheim and Abee are compared with those published by other investigators. Clarke and Thode [8] report substantial variations of the krypton contents and isotopic compositions in different samples of the same meteorite. They show that this could be due to varying amounts of atmospheric contamination adsorbed or occluded in their uncrushed meteorite samples. Also their sample preheating procedure may have led to some gas losses. For the comparison we have chosen those of their results for which simultaneously the concentration and the isotopic composition are known.

Our krypton concentrations agree very well with those of Zähringer [30], whereas the values of Clarke and Thode [8] for Abee 3, 4 and Bruderheim 6

15 G. G. Goles and E. Anders, Geochim. Cosmochim. Acta **26**, 723 [1962].
16 G. W. Reed, K. Kigoshi, and A. Turkevich, Geochim. Cosmochim. Acta **20**, 122 [1960].
17 M. Duke, D. Maynes, and H. Brown, J. Geophys. Res. **66**, 3557 [1961].
18 A. Wyttenbach and H. Dulakas, private communication 1965.
19 A. Wyttenbach, H. R. von Gunten, and W. Scherle, Geochim. Cosmochim. Acta **29**, 467 [1965].
20 C. Rammelsberg, Z. Deutsch. Geol. Gesell. **23**, 734 [1871].
21 R. A. Schmitt, R. H. Smith, and D. A. Olehy, Geochim. Cosmochim. Acta **28**, 67 [1964].
22 G. W. Reed, private communication 1965.
23 R. A. Schmitt, E. Bingham, and A. A. Chodos, Geochim. Cosmochim. Acta **28**, 1961 [1964].
24 G. Merrill, Mem. Nat. Acad. Sci. **14**, 22 [1925].
25 R. A. Schmitt, R. H. Smith, J. E. Lasch, A. W. Mosen, D. A. Olehy, and J. Vasilevskis, Geochim. Cosmochim. Acta **27**, 577 [1963].
26 B. Mason, Am. Museum Novitates No. **2223** [1965].
27 P. W. Gast, J. Geophys. Res. **65**, 1287 [1960].
28 A. DuFresne, Geochim. Cosmochim. Acta **20**, 141 [1960].
29 H. R. von Gunten, A. Wyttenbach, and W. Scherle, Geochim. Cosmochim. Acta **29**, 475 [1965].
30 J. Zähringer, Z. Naturforschg. **17 a**, 460 [1962].

meteorite	reference	Kr^{84} $\times 10^{-12}$ ccSTP/gm	Kr^{78}	Kr^{80}	Kr^{82}	Kr^{83}	Kr^{84}	Kr^{86}
Abee	a	1430	2.03	17.9	68.0	65.7	326	100
Abee 3	b	850	2.01	18.7	68.1	66.1	325	100
Abee 4	b	560	2.09	20.5	69.9	67.2	328	100
Abee	c	1500	—	—	—	—	—	—
Bruderheim	a	157	4.28	20.8	76.5	80.1	335	100
Bruderheim 4	b	160	2.72	15.2	71.6	72.5	332	100
Bruderheim 6	b	16	6.56	27.2	87.7	94.0	347	100
Bruderheim	c	150	—	—	—	—	—	—

meteorite	reference	Xe^{132} $\times 10^{-12}$ ccSTP/gm	Xe^{124}	Xe^{126}	Xe^{128}	Xe^{129}	Xe^{130}	Xe^{131}	Xe^{132}	Xe^{134}	Xe^{136}
Abee	a	610	0.47	0.42	8.52	524	15.7	81.5	100	38.2	32.2
Abee	d	820	0.40	0.36	8.82	636	16.1	81.0	100	38.1	32.0
Abee	c	800	—	—	—	640	—	—	100	—	—
Abee	e	—	—	—	—	530	—	—	100	—	—
Bruderheim	a	99	0.56	0.59	8.29	125.2	15.8	81.8	100	38.6	32.5
Bruderheim	d	250	0.50	0.52	11.7	119.6	16.2	80.4	100	39.2	33.3
Bruderheim	c	130	—	—	—	130	—	—	100	—	—

Table 7. Comparison of our results with published data. References: [a] Present work; [b] CLARKE and THODE [8]; [c] ZÄHRINGER [30]; [d] CLARKE and THODE [6]; [e] JEFFERY and REYNOLDS [31].

are much lower. The isotopic composition of Abee 3 agrees with our results, but Abee 4 shows larger $Kr^{80, 82}$ anomalies. The anomalies in our Bruderheim sample lie between those observed for Bruderheim 4 and 6. The spallation spectra derived from our Bruderheim sample and from Bruderheim 6 are in good agreement with each other (cf. Figure 5).

The agreement between the published xenon concentrations and our results is satisfactory for Abee. In Bruderheim CLARKE and THODE [6] find a 2.5 times higher xenon concentration; the deviation between our and ZÄHRINGER's [30] values lies within the experimental errors. The isotopic composition of the heavier xenon isotopes agrees better for Abee than for Bruderheim. Differences of up to 15% occure for Xe^{124} and Xe^{126} and even more for Xe^{128} of Bruderheim.

5. General Discussion

REYNOLDS and co-workers [1–5] distinguish between the "special anomaly" in the relative abundance of meteoritic Xe^{129} due to radioactive decay of extinct I^{129} and the "general anomalies" which affect the whole spectrum of meteoritic xenon. Krypton had been investigated to a lesser extent until now, and therefore, the general anomalies in its isotopic composition were not as well known. The purpose of the present work is to study the general anomalies of krypton and xenon. Thus, we shall not further discuss the Xe^{129} isotope in our samples.

The following processes may have contributed to the general anomalies of meteoritic krypton and xenon:

1. Mass fractionation due to gravitational, electrostatic or electromagnetic forces (KRUMMENACHER, MERRIHUE, PEPIN and REYNOLDS [2]).
2. Spallation and (n,γ) reactions induced by the exposure of the meteorite to the cosmic radiation during its recent history (MERRIHUE [4]; CLARKE and THODE [8]).
3. In situ production in meteoritic constituents by particle irradiation or spontaneous fission during the early history of the solar system (GOLES and ANDERS [32]; ROWE and KURODA [7]).
4. Addition of products from particle irradiation or fission to the "primordial" Kr and Xe before it became trapped in the meteorite.

It is of course important to remember that not only meteoritic krypton and xenon may have been changed, but that also the isotopic composition of ter-

[31] P. M. JEFFERY and J. H. REYNOLDS, Z. Naturforschg. **16a**, 431 [1961].

[32] G. G. GOLES and E. ANDERS, J. Geophys. Res. **66**, 889 [1961].

restrial krypton and xenon may have been altered by some of these processes (KURODA [33]; CAMERON [34]). In the cases 3 and 4 a multitude of possible reactions has to be considered:

a) Spallation reactions,
b) Special nuclear reactions on Se, Rb, Sr, Te, Cs, Ba etc.,
c) (n,γ) reactions,
d) Spontaneous fission of U^{238} or transuranium elements,
e) Neutron induced fission.

Obviously the effects of such a large number of conceivable processes can only be distinguished with great effort. REYNOLDS and co-workers have successfully applied the method of stepwise heating to establish a number of relations governing the general anomalies of the isotopic abundances of xenon. We have chosen here a different approach and have analyzed selected meteorites, where some of the processes leading to anomalies are strongly enhanced.

6. Spallation Produced Isotopes of Krypton and Xenon

6.1 The Stannern Achondrite

In Figs. 1 and 2 the measured mass spectra of krypton and xenon from the Stannern achondrite are reproduced. As these are original spectra,

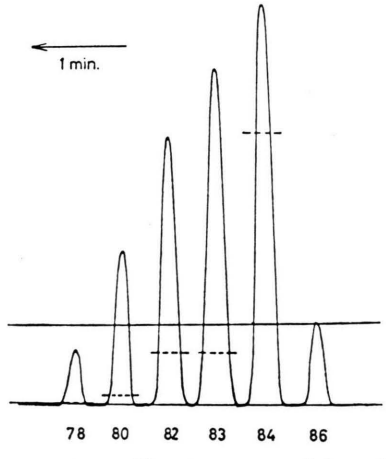

Fig. 1. Mass spectrum of krypton extracted from the Stannern achondrite (original tracing). All isotopes are measured with the same sensitivity. The solid line indicates the decrease of the ion beam intensity with time. The dashed lines correspond to the isotopic composition of atmospheric krypton arbitrarily normalized at Kr^{86}. Increased scanning speed between the peaks was used. The Kr^{86} peak corresponds to 25×10^{-12} cc STP.

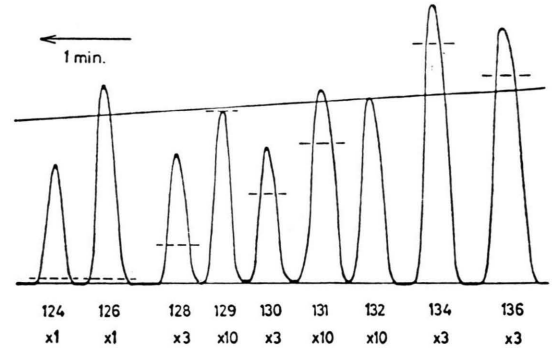

Fig. 2. Mass spectrum of xenon extracted from the Stannern achondrite (original tracing). Scaling factors are indicated below the mass number. The solid line indicates the decrease of the ion beam intensity with time. The dashed lines correspond to the isotopic composition of atmospheric xenon, arbitrarily normalized at Xe^{132}. Increased scanning speed between the peaks was used. The Xe^{124} peak corresponds to 1.5×10^{-12} cc STP.

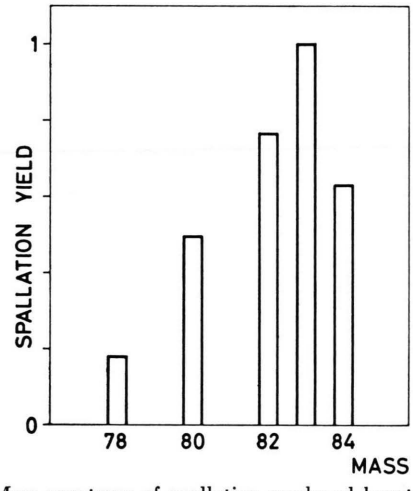

Fig. 3. Mass spectrum of spallation produced krypton as derived from the Stannern meteorite, normalized to $Kr_S^{83}{}_{all} = 1$. For errors see Table 8.

no corrections for blank or discrimination have been applied. The large enrichment of the light Xe and Kr isotopes in this meteorite is evidently due to spallation. It results from a combination of three favorable factors: high abundances of the elements Sr, Y, Zr, Ba, and rare earths which have large spallation cross sections for the production of Kr and Xe isotopes; a relatively high radiation age; and very low abundances of trapped Kr and Xe. Similar, but much smaller enrichments of the light isotopes of Kr and Xe are observed in the H-Ausson and Bruderheim chondrites. In Figs. 3 and 4 and

[33] P. K. KURODA, Nature **187**, 36 [1960].

[34] A. G. W. CAMERON, Icarus **1**, 13 [1962].

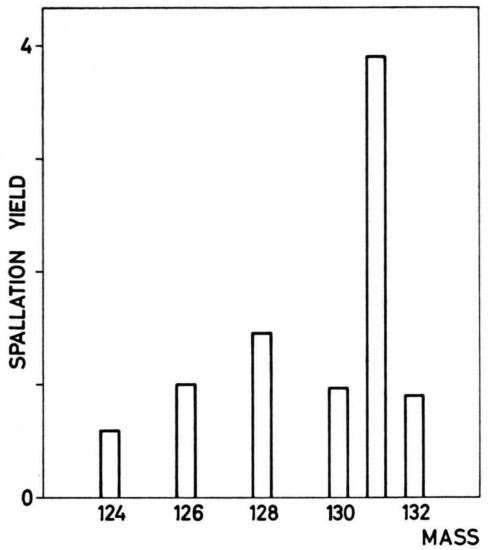

Fig. 4. Mass spectrum of spallation produced xenon as derived from the Stannern meteorite, normalized to $Xe^{126}_{spall} = 1$. For errors see Table 8.

Table 8 the mass spectra of spallation produced Kr and Xe are given. They were calculated from the observed isotopic composition in Stannern with the following considerations:

1. It is assumed that in the Stannern achondrite Xe and Kr consist essentially of three components: spallation, fission and trapped gases. The mixing ratio of these components is unknown and has to be determined.

2. The spallation spectra are unknown. However, it can be assumed that Xe^{136}_{spall} is practically zero, and $(Kr^{86}/Kr^{83})_{spall} \leqq 0.1$. In fact, radiochemical studies of spallation reactions on yttrium, iodine, caesium etc. [35–40] show that spallation products from heavier elements have strong neutron deficiencies. Isotopes occupying similar positions as Xe^{136} or Kr^{86} are hardly produced at all. This tendency becomes more pronounced with growing Z, showing the effect of the rising Coulomb barrier. The resulting low spallation yield for Xe^{134} (cf. Table 8) in fact confirms that the Xe^{136} yield must be very low.

3. The isotopic composition of fission xenon can, of course, not be deduced from the measured xenon spectrum in Stannern, as it is masked by the large and unknown spallation contribution. We may, however, assume that the spectra of the fission components in the Stannern and Pasamonte meteorites are identical. Both are calcium-rich achondrites, but with different radiation ages. Rowe and Kuroda [7] have recently measured the xenon spectrum in Pasamonte and have derived a fission spectrum. They have, however, neglected the spallation component which is much smaller than that in Stannern, but still significant. As the authors do not give Xe^{124} and Xe^{126} abundances the spallation component has to be calculated either from the Xe^{128}/Xe^{130} ratio or from the known radiation age of Pasamonte (cf. chapter 7).

The correction for fission Kr is small and uncertainties in the Kr fission spectrum have little influence on the Kr spallation spectrum. Wetherill's [41] data for the spontaneous fission of U^{238} were taken.

4. For the correction of the trapped gas component, the isotopic composition of Kr and Xe measured in the Mezö-Madaras meteorite was taken. As will be discussed later, Kr^{80}, and to a lesser extent Kr^{82} and Xe^{128} are enriched by (n,γ) reactions in this meteorite relative to carbonaceous chondrites. For these three isotopes the average carbonaceous chondrite abundances were used.

5. The mixing ratio of trapped Xe to fission Xe in Stannern can be derived from the measured Xe^{134}/Xe^{136} ratio. As this ratio is similar in the fission and in the trapped gas component, only rather wide limits for the mixing ratio are obtained. Taking experimenal errors into account and assuming that fission Xe in Stannern and Pasamonte has the same iso-

		Kr^{78}	Kr^{80}	Kr^{82}	Kr^{83}	Kr^{84}		
		0.179 ± 0.008	0.495 ± 0.020	0.765 ± 0.025	1.00	0.63 ± 0.17		
Xe^{124}	Xe^{126}	Xe^{128}	Xe^{130}	Xe^{131}	Xe^{132}	Xe^{134}	$\frac{Xe^{128}}{Xe^{130}}$	$\frac{Xe^{131}}{Xe^{130}}$
0.590 ± 0.015	1.00	1.45 + 0.25 − 0.12	0.97 + 0.50 − 0.25	3.9 + 2.5 − 1.1	0.9 + 2.3 − 0.9	≦ 0.25	1.50 ± 0.35	4.0 ± 0.2

Table 8. Isotopic composition of spallation produced krypton and xenon as derived from the Stannern meteorite.

[35] J. M. Miller and J. Hudis, Ann. Rev. Nucl. Sci. **9**, 159 [1959].
[36] B. G. Harvey, in Progress in Nuclear Physics (O. R. Frisch ed.), Pergamon Press, London 1959, p. 89.
[37] A. A. Caretto and E. O. Wiig, Phys. Rev. **103**, 236 [1956].
[38] J. H. Coleman and H. A. Tewes, Phys. Rev. **99**, 288 [1955].
[39] R. W. Fink and E. O. Wiig, Phys. Rev. **96**, 185 [1954].
[40] L. Winsberg, Phys. Rev. **95**, 198 [1954].
[41] G. W. Wetherill, Phys. Rev. **92**, 907 [1953].

topic composition, one obtains $0.3 \leqq Xe^{136}_{fission}/Xe^{136} \leqq 1$. A better upper limit for the $Xe^{136}_{fission}$ content can be obtained from the concentration of trapped krypton. A survey of all the available data on trapped gases shows that trapped Xe in most meteorites is more abundant than trapped Kr (PEPIN and SIGNER [42, 43]). In meteorites with solar-type trapped gases the lowest $(Xe/Kr)_{trapped}$ ratio observed is 0.3. No indication for solar type trapped gases is found in Stannern. For planetary-type trapped gases the lowest $(Xe/Kr)_{trapped}$ ratio observed is 0.7. Using this figure as lower limit for Stannern, one obtains $Xe^{136}_{fission}/Xe^{136} \leqq 0.8$. An upper limit for $Kr^{86}_{fission}/Kr^{86}$ of 0.12 in Stannern is obtained from the Kr/Xe ratio of U^{238} spontaneous fission [41]. If the fission component in Stannern had resulted from spontaneous fission of transuranium elements, the fission ratio Kr/Xe would probably be smaller. Thus, $Kr^{86}_{fission}/Kr^{86} \leqq 0.12$ is assumed.

It should be pointed out that the relative spallation production rates of the *light* isotopes of Kr and Xe are quite independent of all these assumptions. This is reflected in their small errors. Especially the Xe^{126}/Xe^{124} ratio is virtually not influenced by any possible correction.

Xe^{130} has a relatively low spallation yield. This is due to partial shielding by Ba^{130} and reflects the strong neutron deficiency in heavy spallation products.

6.2 *Spallation Isotopes in Chondrites*

The Kr and Xe spallation components in the chondrites H-Ausson and Bruderheim can be deduced in the same way. For xenon only Xe^{124}_{spall} and Xe^{126}_{spall} can be determined with sufficient accuracy. We have corrected these two isotopes with the Xe composition of Mezö-Madaras.

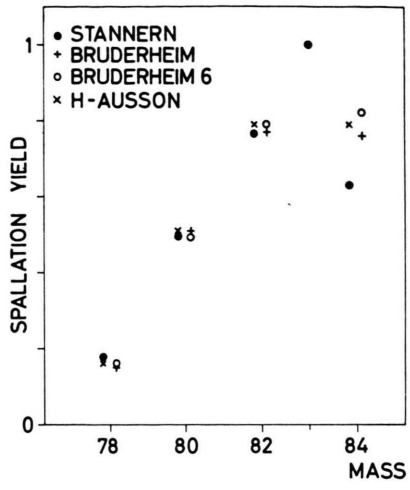

Fig. 5. Comparison of the mass spectra of spallation krypton in three meteorites. Bruderheim 6 from CLARKE and THODE [8], all the others from the present work.

$(Xe^{124}/Xe^{126})_{spall}$ ratios are given in Table 9. The agreement between the three meteorites is very good.

A comparison between the Kr spallation spectra in Stannern, H-Ausson and Bruderheim is given in Fig. 5. The average isotopic composition of krypton from carbonaceous chondrites was assumed for the correction for trapped krypton. Included is also a spallation spectrum derived from the Kr anlysis of Bruderheim 6 by CLARKE and THODE [8]. The agreement is generally good.

In Table 9 the concentrations of some spallation isotopes of argon, krypton and xenon are compared. It is evident that the concentrations of the Xe and Kr spallation isotopes rise with increasing radiation

meteorite	radiation age 10^6 yrs.	Ar^{38}_{spall} 10^{-8} cc/gm	Kr^{82}_{spall} 10^{-12} cc/gm	Xe^{126}_{spall} 10^{-12} cc/gm	$\left(\frac{Xe^{126}}{Ar^{38}}\right)_{spall}$	$\left(\frac{Xe^{126}}{Kr^{82}}\right)_{spall}$	$\left(\frac{Xe^{126}}{Xe^{124}}\right)_{spall}$
H-Ausson	50	3.1[a]	8.5	0.30	1.0×10^{-5}	0.035	1.7
Bruderheim	26	1.44[a]	5.7	0.19	1.3×10^{-5}	0.033	1.65
Average chondrite, spallation theory					2.6×10^{-5}	0.058	
Stannern	~ 30	5.15[b]	31	3.1	6×10^{-5}	0.10	1.70 ± 0.05
Stannern, spallation theory					12×10^{-5}	0.11	

Table 9. Concentrations of some spallation produced isotopes in three meteorites. Concentrations of the other spallation isotopes can be calculated from ratios given in Table 8. For comparison ratios of spallation isotopes calculated from general spallation theory [Eq. (3)] are given. References: [a] EBERHARDT, EUGSTER, GEISS, and MARTI [13]; [b] KIRSTEN, KRANKOWSKY, and ZÄHRINGER [12].

[42] R. O. PEPIN and P. SIGNER, Science **149**, 253 [1965].

[43] Contrary to PEPIN and SIGNER [42], we assume that the excess Xe^{129} does not belong to the trapped component.

age. The higher concentrations in Stannern reflect the greater abundances of Sr, Zr, Ba, and the rare earth elements in this meteorite. This pattern strongly suggests that the spallation components of Xe and Kr in the three meteorites were produced by the same radiation as were He^3, Ne^{21} and Ar^{38}, i. e. they are due to cosmic ray bombardment late in the history of the solar system. In the following this will be discussed in a more quantitative way.

6.3 Comparison between Observed and Calculated Spallation Yields

The excitation function for spallation reactions can be approximated by [44–46]

$$\sigma(E, A_0, \Delta A) = \sigma_0 A_0^{2/3} c E^{-2/3} \exp[-c E^{-2/3} \Delta A] \quad (1)$$

with $$c = \frac{0.25}{1+0.022 A_0} \text{GeV}^{2/3}, \quad \sigma_0 = 60 \text{ mb}.$$

A_0 is the atomic number of the target nucleus and ΔA the total mass loss. Assuming an irradiation spectrum of the form

$$f(E)\, dE = f_0 E^{-\alpha}\, dE \quad (2)$$

and upon integrating, one obtains for the production rate of an isobar [47]

$$P(\Delta A, A_0) = B \cdot (\Delta A)^{-n} \quad (3)$$

with $B = \frac{3}{2} \sigma_0 A_0^{2/3} f_0 \Gamma(n)/c^{n-1}$, $n = \frac{1}{2}(3\alpha - 1)$.

Equation (3) has been successfully applied to iron meteorites with Fe as target [47, 48], as well as to other target elements in meteorites [49]. The parameter n depends on the hardness of the irradiation and can be calculated if the ΔA distribution of spallation isotopes has been measured. Values of $n = 2.0$ for small iron meteorites rising to $n = 2.6$ for large ones have been obtained [47, 48, 50]. No experimental data exist for stone meteorites. However, most stone meteorites are small and we have chosen $n = 2$ for all three meteorites.

$P(\Delta A, A_0)$ is the production rate for the total isobar. It has to be multiplied by the isobaric fraction coefficient g in order to obtain the cross section for one nucleus. We shall explicitly calculate production rates for Ar^{38}, Kr^{82} and Xe^{126}. For Ar^{38} and Kr^{82} $g = 1$. For Xe^{126} $g = 0.8$ is estimated from radiochemical spallation data [35–40].

Equation (3) has to be summed over all target nuclei in the meteorite. The chemical abundances given in Table 6 are used. Ar^{38} is mainly produced from Ca and Fe; Kr^{82} from Sr, Zr and Y; and Xe^{126} from Ba and the rare earth elements.

The spallation formula (3) breaks down for $\Delta A \lesssim 5$, i. e. for $Rb \rightarrow Kr^{82}$ and $Ca \rightarrow Ar^{38}$. We therefore take

$$\sigma(Ca \rightarrow Ar^{38}) = 11.8 \times \sigma(Fe \rightarrow Ar^{38})$$

from Stauffer's [11] work and assume

$$\sigma(Rb \rightarrow Kr^{82}) = \sigma(Sr \rightarrow Kr^{82}).$$

Production rates calculated from Eq. (3) are given in Table 9. They are estimated to be correct only within a factor of two, in view of the wide range in A_0 and ΔA to which the very simple spallation formula (3) is being applied. Thus, the agreement between experimentally observed and theoretical ratios of spallation isotopes is quite satisfactory.

For practical purposes the production rates of Ar^{38}, Kr^{83} and Xe^{126} can be approximately calculated from the simple relations

$$Ar^{38}_{spall} = \varkappa T_r([Fe] + a[Ca]), \quad (4)$$

$$Kr^{83}_{spall} = \varkappa T_r(b[Sr] + c[Y] + d[Zr]), \quad (5)$$

$$Xe^{126}_{spall} = \varkappa T_r(e[Ba] + f[REE]), \quad (6)$$

and

$$\left(\frac{Xe^{126}}{Ar^{38}}\right)_{spall} = \frac{e[Ba]+f[REE]}{[Fe]+a[Ca]}, \quad (7)$$

$$\left(\frac{Xe^{126}}{Kr^{83}}\right)_{spall} = \frac{e[Ba]+f[REE]}{b[Sr]+c[Y]+d[Zr]} \quad (8)$$

with
$a = 16.5$, $d = 3.2$,
$b = 10$, $e = 1.25$,
$c = 5.9$, $f = 0.45$,
$\varkappa = 0.12 \times 10^{-8}$ cc STP/m. y. gm

T_r : radiation age,
[Fe] = concentrations of Fe + Ni + Co + Mn + Cr + V,
[Ca] = concentrations of Ca + K + Sc + Ti,
[Sr] = concentrations of Sr + Rb,
[Y] = concentration of Y,
[Zr] = concentrations of Zr + Nb + Mo,
[Ba] = concentrations of Ba + Cs,
[REE] = concentrations of elements La to Lu.

[44] G. Rudstam, Thesis, University of Uppsala 1956.
[45] M. Honda and D. Lal, Phys. Rev. **118**, 1618 [1960].
[46] H. Oeschger and U. Schwarz, unpublished calculations, 1961.
[47] J. Geiss, H. Oeschger, and U. Schwarz, Space Sci. Rev. **1**, 197 [1962].
[48] H. Stauffer and M. Honda, J. Geophys. Res. **67**, 3503 [1962].
[49] F. Begemann, Z. Naturforschg. **20 a**, 950 [1965].
[50] H. Voshage, Z. Naturforschg. **17 a**, 422 [1962].

meteorite	Xe^{126}_{spall}		$(Xe^{126}/Ar^{38})_{spall}$		$(Xe^{126}/Kr^{83})_{spall}$	
	measured 10^{-12} cc/gm	Eq. (6) 10^{-12} cc/gm	measured 10^{-5}	Eq. (7) 10^{-5}	measured	Eq. (8)
Bruderheim	0.19	0.18	1.32	1.22	0.026	0.031
H-Ausson	0.30	0.35	0.97	1.11	0.028	0.032
Stannern	3.1	2.7	6.0	5.7	0.077	0.061

Table 10. Comparison of measured Xe^{126}_{spall} concentrations and $(Xe^{126}/Ar^{38})_{spall}$ and $(Xe^{126}/Kr^{83})_{spall}$ ratios with figures calculated according to Eqs. (6), (7), and (8).

The value for a is taken from STAUFFER [11]; $c/b = 0.59$, $d/b = 0.32$, and $f/e = 0.36$ are calculated from Eq. (3), b and e are averages obtained from the observed $(Xe^{126}/Ar^{38})_{spall}$ and $(Xe^{126}/Kr^{83})_{spall}$ ratios in H-Ausson, Bruderheim and Stannern. $\varkappa$ is based on H^3/He^3 radiation ages and He^3/Ar^{38}_{spall} ratios [13]. Variations in the size of the meteorite should influence Eqs. (7) and (8) less than Eqs. (4), (5), and (6).

In Table 10 Xe^{126}_{spall} concentrations and $(Xe^{126}/Ar^{38})_{spall}$ and $(Xe^{126}/Kr^{83})_{spall}$ ratios calculated from Eqs. (6), (7) and (8) are compared with the measured values. The agreement is satisfactory.

6.4 Conclusions

All these observations on the Kr and Xe spallation fractions in the three meteorites H-Ausson, Bruderheim and Stannern can be summarized as follows:

1. The spectra obtained are typical for spallation products from heavy elements.
2. The concentrations are proportional to radiation ages.
3. The concentrations vary according to chemical abundances.
4. The production rates are in agreement with general spallation theory.

We may, thus, safely accept that the irradiation responsible for the production of Ar^{38}_{spall}, Ne^{21}_{spall} and He^3_{spall} can fully account for the Kr and Xe spallation components observed in the three meteorites. It is generally agreed that the light spallation isotopes have been produced by cosmic radiation after the meteorite was removed from a shielded location inside its parent body late in its history. Consequently, this is also true for spallation Xe and Kr observed in the three meteorites discussed here.

A survey of the literature shows that *so far* all the observed Xe^{124} and Xe^{126} anomalies, which are higher than the carbonaceous chondrite abundances, can be interpreted as arising from a mixture of

a) primordial Xe as observed in carbonaceous chondrites; and
b) spallation xenon produced by cosmic radiation late in the history of the meteorite.

Until now the most extreme Xe^{124} and Xe^{126} anomalies were those observed by MERRIHUE [4] in separated chondrules of Bruderheim. The Xe^{126} excess, when corrected for meteoritic trapped xenon, is 0.2×10^{-12} cc STP/gm, which is very close to our figure of 0.19×10^{-12}cc STP/gm observed in the whole meteorite (Table 9).

7. Fission Xenon

ROWE and KURODA [7] have found a fission component in the Pasamonte achondrite, corresponding to $Xe^{136}_{fission} = 3 \times 10^{-12}$ cc STP/gm. In Stannern a similar fission component is detectable. However, because of the larger concentration of spallation isotopes the fission component can only be determined approximately in this meteorite. As outlined in chapter 6.1, $Xe^{136}_{fission}$ in Stannern lies between 3 and 8×10^{-12} cc STP/gm. If the xenon in the chondrites H-Ausson and Bruderheim is compared with that in Mezö-Madaras or other meteorites containing large amounts of Xe, it is evident that the excess fission component, if at all present, is about one order of magnitude smaller. Thus, a correlation of this component with U is apparent. As pointed out by ROWE and KURODA [7], however, spontaneous fission of U^{238} cannot account for the observed fission xenon concentrations in calcium-rich achondrites by one order of magnitude, and spontaneous fission of extinct transuranium isotopes, such as Pu^{244} ($T_{1/2} = 75$ m. y.), is implied. The correlation with the uranium content would then result from the geochemical affinity of U and Pu.

Rowe and Kuroda [7] have derived a spectrum for the fission xenon in Pasamonte neglecting, however, the spallation component. Even for the short radiation age of Pasamonte this introduces an appreciable error and we have recalculated the xenon fission spectrum in this meteorite using the spallation spectrum obtained in this paper. The Xe^{124} and Xe^{126} abundances are not known for Pasamonte. Therefore, the spallation contribution has to be calculated from the radiation age [52, 53] [applying Eq. (6)] or from the observed Xe^{128}/Xe^{130} ratio. Both methods give virtually the same fission spectrum. The choice of the isotopic composition for the trapped component is not critical. Correcting with either average carbonaceous chondrite (AVCC [2]) xenon or terrestrial xenon leads to very similar xenon fission spectra as can be seen from Fig. 6. The indicated errors include the experimental errors as well as the uncertainties in the spallation concentration and spectrum.

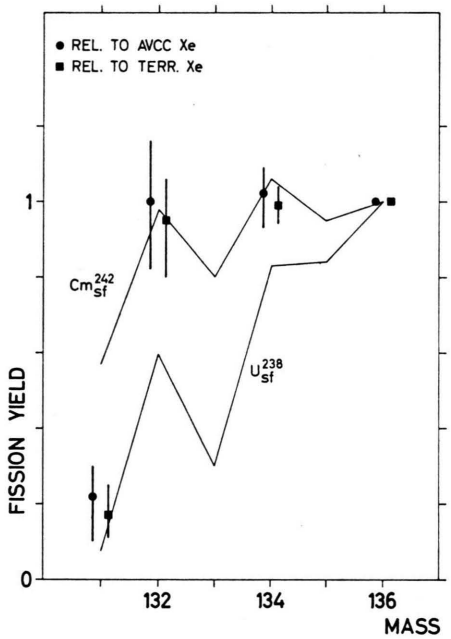

Fig. 6. Mass spectrum of fission xenon as derived from Rowe and Kuroda's [7] measurement of the Pasamonte achondrite. The spallation component has been corrected for. $Xe^{130}_{fission}$ was assumed to be zero. Solid circles: AVCC−Xe isotopic composition assumed for the trapped component (relative fission yields $Xe^{136}=1.00$; $Xe^{134}=1.02^{+0.07}_{-0.09}$; $Xe^{132}=1.00^{+0.16}_{-0.18}$; $Xe^{131}=0.22^{+0.08}_{-0.12}$). Solid squares: terrestrial xenon isotopic composition assumed for the trapped component (reraltive fission yields $Xe^{136}=1.00$; $Xe^{134}=0.99\pm0.05$; $Xe^{132}=0.95^{+0.11}_{-0.15}$; $Xe^{131}=0.17^{+0.08}_{-0.06}$). For comparison the spontaneous fission yield curves for U^{238} and Cm^{242} are given [51].

The xenon fission spectrum obtained from Pasamonte is different from that of U^{238} and Cf^{252} spontaneous fission, and also of U^{235} slow neutron induced fission [51]. The high yield for mass 132 is in agreement with the Cm^{242} yield curve. A high Xe^{132} spontaneous fission yield is also expected from 75 m. y. Pu^{244} because of the influence of double magic Sn^{132} (Cameron [34]).

The spectrum we obtain for meteoritic fission xenon is remarkably similar to that in the Navajo natural gas [6].

8. Trapped Gases

8.1 Trapped Xenon

The isotopic composition of xenon in meteorites containing large quantities of heavy noble gases is listed in Table 11. The AVCC (average carbonaceous chondrite) figures are averages from analyses of Murray, Mighei, and Orgueil [2]. Enstatite chondrites not listed (Indarch, St. Mark's [2]) have Xe isotopic ratios similar to Abee. Reynolds and Turner [54] have extensively studied Xe in the Renazzo chondrite and have shown that it contains at least three components. They may be described as follows:

1. Xe evolved at 200 – 400 °C having an isotopic composition somewhere between carbonaceous chondrites and the atmosphere.
2. Xe released at 500 – 1300 °C having an isotopic composition close to that of carbonaceous chondrites.
3. Fission xenon.

The component 3. is included in the 500 – 1300 °C fraction in Table 11. Because of the rather high abundance of the low temperature component Reynolds and Turner [54] have concluded that its isotopic composition cannot be explained by terrestrial contamination. It is interesting to speculate that part of this component might be "solar type" trapped gas, whereas Xe released at higher temperature

[52] J. Geiss and D. C. Hess, Astrophys. J. **127**, 224 [1958].
[53] P. Eberhardt and D. C. Hess, Astrophys. J. **131**, 38 [1960].
[51] E. K. Hyde, Lawrence Radiation Laboratory Report No. 9036 [1960].
[54] J. H. Reynolds and G. Turner, J. Geophys. Res. **69**, 3263 [1964].

meteorite	Xe^{132} 10^{-12} ccSTP/gm	Xe^{124}	Xe^{126}	Xe^{128}	Xe^{130}	Xe^{131}	Xe^{132}	Xe^{134}	Xe^{136}
Atmosphere[a]		0.357	0.335	7.14	15.2	78.8	100	38.8	33.0
AVCC[b]		0.486	0.439	8.30	16.2	82.0	100	38.2	32.2
Renazzo[c] 200—400 °C	830	0.39	0.35	7.47	15.5	79.7	100	38.5	32.6
500—1300 °C	2600	0.464	0.413	8.20	16.3	81.9	100	38.4	32.5
Mezö-Madaras[d]	2050	0.455	0.411	8.39	15.9	81.4	100	38.0	32.0
Abee[d]	612	0.468	0.416	8.51	15.7	81.5	100	38.2	32.2

Table 11. Xe isotopic composition of xenon-rich meteorites (AVCC=average carbonaceous chondrites). Mezö-Madaras and Abee have been corrected for cosmic ray induced spallation. Data from: [a] NIER [14]; [b] KRUMMENACHER, MERRIHUE, PEPIN, and REYNOLDS [2]; [c] REYNOLDS and TURNER [54]; [d] Present work.

	Xe^{124}	Xe^{126}	Xe^{128}	Xe^{130}	Xe^{131}	Xe^{132}	Xe^{134}	Xe^{136}
Atmosphere	1.00	0.94	20.0	42.6	231	280	108.7	92.4
AVCC	1.00	0.90	17.1	33.3	169	206	78.6	66.3
17% Atm. + 83% AVCC	1.00	0.91	17.6	34.9	178	219	83.7	70.7
Mezö-Madaras	1.00	0.90	18.4	34.9	179	220	83.5	70.3
8% Atm. + 92% AVCC	1.00	0.90	17.3	34.0	173	212	81.0	68.4
Abee	1.00	0.89	18.2	33.6	174	214	81.6	68.8

Table 12. Comparison of xenon isotopic composition (corrected for spallation) of Mezö-Madaras and Abee with mixtures of AVCC and atmospheric xenon. Normalization to Xe^{124} is used (c. f. chapter 8.2). The agreement is satisfactory except for Xe^{128}, where an excess due to $I^{127}(n,\gamma\beta)Xe^{128}$ is observed in both meteorites.

constitutes the "planetary type". This would be consistent with the observation that solar type trapped gases are located at the surfaces of the individual grains in the meteorite [55–57].

Also the trapped xenon in Mezö-Madaras and Abee seems to be a mixture of AVCC-xenon and xenon of atmospheric composition as can be seen from Table 12. The agreement between the assumed mixtures and the trapped xenon is well within the experimental errors, except for an excess of Xe^{128}. This excess will be discussed in chapter 9.

8.2 Atmospheric and Meteoritic Xenon

Several possible mechanisms have been suggested in order to explain the large differences between the isotopic composition of atmospheric xenon and AVCC-xenon: 1) Trapped xenon in meteorites contains a spallation fraction [32]; 2) Mass fractionation and addition of fission xenon to meteoritic xenon [2]; 3) Nuclear reactions on Te [2]; 4) Addition of fission xenon [33] and (n,γ) products to atmospheric xenon [34]; 5) Mass fractionation in the terrestrial atmosphere.

We have shown in chapter 6.1 that in cosmic ray induced spallation the Xe^{126}/Xe^{124} ratio is 1.70 ± 0.05. This ratio will increase if spallation is induced by particles of lower energy. It might decrease somewhat if the effective irradiation energy is higher than it was in the Stannern meteorite. A large decrease, however, cannot be expected. In order to explain the difference between atmospheric and AVCC-xenon solely by the addition of a spallation fraction to the latter, a ratio $(Xe^{126}/Xe^{124})_{spall} = 0.8 \pm 0.2$ would be required. This seems to be ruled out by our observation on Stannern. Reactions of deuterons on Te give small yields for Xe^{124} and cannot be used as an explanation for the difference between atmospheric and meteoritic Xe [2]. α-particle reactions may still be a possibility, and also of course mass fractionation. But at present it seems reasonable to assume that the light Xe isotopes Xe^{124} and Xe^{126} have been affected relatively little by nuclear reactions or transformations and therefore can be useful for normalization (cf. Table 12).

9. The Kr^{80}, Kr^{82}, and Xe^{128} Anomalies

Table 13 gives a comparison of the krypton isotopic composition of meteorites with large quantities

[55] P. EBERHARDT, J. GEISS, and N. GRÖGLER, Tschermaks Mineral. Petrogr. Mitt., 3. Folge, **10**, 535 [1965].

[56] H. HINTENBERGER, E. VILCSEK, and H. WÄNKE, Z. Naturforschg. **20 a**, 939 [1965].

[57] P. EBERHARDT, J. GEISS, and N. GRÖGLER, J. Geophys. Res. **70**, 4375 [1965].

meteorite	Kr 10^{-12} ccSTP/gm	Kr^{78}	Kr^{80}	Kr^{82}	Kr^{83}	Kr^{84}	Kr^{86}
Atmosphere[a]		2.04	13.1	66.6	66.5	327.6	100
Orgueil[b]	9000	—	12.9 ± 0.2	65.0 ± 0.7	65.3 ± 0.8	323 ± 2	100
Murray[b]	7000	2 ± 0.2	12.9 ± 0.2	65.2 ± 1.0	65.5 ± 1.0	326 ± 5	100
AVCC		2	12.9	65.1	65.4	324	100
Abee 3[c]	1500	1.91 ± 0.06	18.4 ± 0.4	67.7 ± 0.5	65.5 ± 0.6	325 ± 3	100
Abee 4[c]	1000	1.94 ± 0.12	20.1 ± 0.5	69.3 ± 1.3	66.3 ± 1.3	327 ± 3	100
Abee[d]	2550 ± 300	1.97 ± 0.06	17.7 ± 0.2	67.8 ± 0.6	65.4 ± 0.5	326 ± 2	100
Mezö-Madaras[d]	5300 ± 800	1.88 ± 0.10	17.3 ± 0.2	67.5 ± 0.8	65.0 ± 0.7	326 ± 2	100

Table 13. Kr isotopic composition (corrected for spallation) in meteorites with large amounts of trapped heavy noble gases. AVCC: average carbonaceous chondrite (weighted average from Murray and Orgueil). References: [a] Nier [14]; [b] Krummenacher, Merrihue, Pepin, and Reynolds [2]; concentration from Zähringer[30]; [c] Clarke and Thode [8]; [d] Present work.

of trapped heavy noble gases. Listed are all analyses in which at least one of the two light isotopes Kr^{78} and Kr^{80} has been measured. The AVVC-krypton (weighted average from Murray and Orgueil) is identical within the limits of error with terrestrial krypton, except for a possible slight excess of Kr^{86} (Krummenacher et al. [2]). The most conspicious feature, however, is the large difference in the Kr^{80} abundance between the carbonaceous chondrites, on one hand, and Mezö-Madaras and Abee on the other. This cannot be due to spallation reactions because of the very different nature of the krypton spallation spectrum (cf. Fig. 3). Clarke and Thode [8] have already pointed out that neutron capture by bromine is the most likely explanation. This could have occurred either in situ by the meteoritic bromine or by bromine not associated with the meteorite. In the latter case the krypton formed would have been added to the trapped krypton found in the meteorite.

For the discussion of the origin of this Kr^{80} excess and the possibility of an in situ production it is useful to define absolute excesses

$$E_M^{(84)} = \left[\left(\frac{Kr^M}{Kr^{84}}\right)_{\text{meteorite}} - \left(\frac{Kr^M}{Kr^{84}}\right)_{\text{AVCC}}\right] Kr^{84}_{\text{meteorite}} \quad (9)$$

These epsilon-values are given in Table 14. The absolute Kr^{80} excess is largest in Mezö-Madaras. It is approximately twice as large in our Abee sample as it is in those of Clarke and Thode [8]. If the $Br^{79}(n,\gamma\beta)Kr^{80}$ reaction is responsible for this Kr^{80} anomaly then the same neutrons should also produce other isotopes, e. g. $Br^{81}(n,\gamma\beta)Kr^{82}$, $I^{127}(n,\gamma\beta)Xe^{128}$, $Cl^{35}(n,\gamma\beta)Ar^{36}$. The presence or absence of an excess in these isotopes will be a crucial test for the neutron capture hypothesis and also for a possible in situ production.

meteorite	$E_M^{(84)} \times 10^{-12}$ cc STP/gm 78	80	82	83	86	$E_{128} \times 10^{-12}$ cc STP/gm
Abee 3	—	14 ± 2	6 ± 3	0 ± 3	-1 ± 4	—
Abee 4	—	12 ± 2	6 ± 3	1 ± 3	-2 ± 3	—
Abee	—	21 ± 2	10 ± 5	-2 ± 4	-3 ± 5	2.5 ± 1
Mezö-Madaras	—	40 ± 4	18 ± 11	-7 ± 10	-6 ± 10	7.5 ± 4

Table 14. Krypton and Xe^{128} excess concentrations in the Abee and Mezö-Madaras meteorites. Abee 3 and 4 data from Clarke and Thode [8]. Abee and Mezö-Madaras this paper. Krypton excesses $E_M^{(84)}$ calculated from Table 12 according to Eq. (9), Xe^{128} excesses E_{128} from Table 11. Concentration errors are not included because they are systematic.

Table 14 shows Kr^{82} excesses outside of the experimental errors for Mezö-Madaras and for all Abee samples. These Mezö-Madaras and Abee samples show also a Xe^{128} excess, as can be seen from Tables 12 and 14. The Ar^{36}/Ar^{38} ratio in Mezö-Madaras[13] does not show an Ar^{36} anomaly due to $Cl^{35}(n,\gamma\beta)Ar^{36}$, and only an upper limit can be given for neutron produced Ar^{36}.

In order to estimate possible relative production rates for different isotopes by (n,γ) processes, we shall calculate the production in three different energy regions: 1) E_{th} to ~ 10 eV (σ_a roughly $\sim 1/v$); 2) $30 - 300$ eV (σ_a determined by several large resonances); and 3) 10 keV – 100 keV (σ_a roughly $\sim 1/E$). The three energy regions sufficiently cover the possible neutron spectra, namely 1) highly moderated, 2) moderated, 3) poorly moderated.

In the first region it is assumed that $\sigma_a \sim 1/v$ for all isotopes, in fairly good agreement with experimental data. The resonance integral R is then

$$R = \int_{E_{th}}^{\infty} \sigma_a \frac{dE}{E} = 2\,\sigma_{th}\,. \tag{10}$$

In the second region, resonance integrals

$$R = g \frac{\hbar^2}{4\,m_N} \frac{\Gamma_n \Gamma_\gamma}{E_0^2\,\Gamma} \tag{11}$$

have to be determined for each resonance in the region and added. The statistical factor g is taken as 1/2. E_0, the resonance energy, and Γ_n, Γ_γ and Γ, the neutron, gamma and total widths respectively are taken from BNL 325 [58] for Br^{79}, Br^{81} and I^{127}. For Cl^{35} R is calculated from measurements of KASHUKEEV, POPOV, and SHAPIRO [59]. The values for Se^{82} and Te^{130} are based on TRURAN's [60] calculations. TRURAN has also obtained cross sections for Br^{79}, Br^{81}, and Cl^{35} which are in satisfactory agreement with the values of BNL 325 [58] and KASHUKEEV et al. [59]. In the third energy region R is based on measured $\sigma(n,\gamma)$ cross sections [58, 59] and on TRURAN's [60] theoretical calculations.

target	$R = 2\,\sigma_{th}$ (E_{th} − 10 eV) barn	R (30−300 eV) barn	R (10−100 keV) barn
Cl^{35}	89 [a]	0.6 [b,c]	0.04 [b,c]
Br^{79}	23 [a]	110 [a]	1.3 [a,c]
Br^{81}	6.6 [a]	42 [a]	0.8 [a,c]
Se^{82}	0.11 [a]	1 [c]	0.04 [c]
I^{127}	11 [a]	130 [a]	2 [a]
Te^{130}	0.46 [a]	1.2 [c]	0.05 [c]

Table 15. Resonance integrals $R = \int \sigma_a (dE/E)$ in three neutron energy intervals for some relevant isotopes. Data from: [a] BNL 325 [58]; [b] KASHUKEEV, POPOV, and SHAPIRO [59]; [c] TRURAN [60].

Table 15 gives the resonance integrals for some relevant nuclei. In Table 16 the concentrations, which should result from (n,γ) reactions in Abee and Mezö-Madaras, are calculated in the three neutron energy regions. The theoretical concentrations are normalized to the observed Kr^{80} excesses. Also given are the integrated neutron slowing down densities required to produce the observed Kr^{80} excesses. They are calculated from

$$N = R \cdot Q/(\xi\,\Sigma_{tot}) \tag{12}$$

assuming constant slowing down density within the energy region in question. N is the number of atoms/cm³ produced per target atom and $\xi\,\Sigma_{tot}$ is 3.54×10^{-2} cm^{-1} for ordinary chondritic material [61].

neutron produced isotope	excess observed 10^{-12} cc STP/gm	theoretical (n,γ) production 10^{-12} cc STP/gm		
		E_{th}−10 eV	30−300 eV	10−100 keV
Abee				
Kr^{80}	21	21	21	21
Kr^{82}	10	6	8	13
Xe^{128}	2.5	0.5	1.3	1.7
Ar^{36}	—	4.2×10^4	60	340
Kr^{83}	<2	0.08	0.15	0.5
Xe^{131}	<12	0.12	0.06	0.2
required Q neutrons/cm³		6.6×10^{13}	1.4×10^{13}	1.2×10^{15}
MezöMadaras				
Kr^{80}	40	40	40	40
Kr^{82}	18	11	15	25
Xe^{128}	7.5	2	5	7
Ar^{36}	$<3 \times 10^4$	1.5×10^5	200	1200
Kr^{83}	<3	0.8	1.5	5
Xe^{131}	<40	0.4	0.25	0.8
required Q neutrons/cm³		1.1×10^{15}	2.3×10^{14}	1.9×10^{16}

Table 16. Comparison of observed excess isotopic abundances with calculated (n,γ) production. The latter have been normalized to the observed Kr^{80} excess. Also given are the integrated neutron slowing down densities Q required to produce the observed Kr^{80} excess in each interval. Average hypersthene chondrite chemical composition has been assumed for Mezö-Madaras.

Thermal or slow neutrons ($E < 10$ eV) cannot account for the observed Kr^{80} excess for two reasons: a) the predicted Ar^{36} excess is not observed in Mezö-Madaras; b) a situation where the slowing down density is much higher at E_{th} to 10 eV than it is at 30 to 300 eV is very unlikely in nature. Thus, intermediate or fast neutrons must be responsible for the Kr^{80} anomaly, and quite possibly a considerable fraction is produced by the resonances in the 30 to 300 eV region. The production ratio

[58] Neutron Cross Sections, compiled by D. J. HUGHES and R. B. SCHWARTZ, BNL 325 second edition [1958] and Supplement No. 1 [1960].

[59] N. T. KASHUKEEV, YU. P. POPOV, and E. L. SHAPIRO, J. Nucl. Energy, parts A and B, **14**, 76 [1961].

[60] J. W. TRURAN, unpublished calculations based on the method given by J. W. TRURAN, C. J. HANSEN, A. G. W. CAMERON, and A. GILBERT, Thermonuclear Reaction Rates in Medium and Heavy Nuclei (preprint 1965).

[61] P. EBERHARDT, J. GEISS, and H. LUTZ, in Earth Science and Meteoritics, dedicated to F. G. HOUTERMANS (J. GEISS and E. D. GOLDBERG ed.), North Holland Publ. Co., Amsterdam 1963, p. 143.

Kr^{80}/Kr^{82} would then be approximately 2.5, in excellent agreement with the observed $(Kr^{80}/Kr^{82})_{excess}$ ratios (cf. Table 14). Also the calculated $(Xe^{128}/Kr^{80})_{excess}$ ratios are in satisfactory agreement with the observed Xe^{128} excesses. Therefore, no doubt remains that the Kr^{80}, Kr^{82} and Xe^{128} excesses given in Table 14 are indeed due to (n,γ) reactions of medium energy or fast neutrons.

9.1 Sources of Neutrons

During the exposure of the meteorite to the cosmic radiation, secondary neutrons are produced in the nuclear interactions. These neutrons are then moderated inside the meteorite. EBERHARDT, GEISS, and LUTZ [61] have extensively treated this problem and calculated slowing down densities of comic ray produced neutrons in stone meteorites. In small meteorites virtually all the neutrons escape and therefore slowing down densities are strongly size dependent.

In order to obtain the Q-values given in Table 16 during the radiation age of the meteorites slowing down densities of $q' = 0.07$ neutrons cm^{-3} sec^{-1} for Abee and $q' = 0.28$ neutrons cm^{-3} sec^{-1} for Mezö-Madaras would be required in the energy range of 30 eV to 300 eV. Such slowing down densities only occur in meteorites (spherical shape) with radii larger than 30 cm and 55 cm respectively. These limits may be $10-20\%$ too high, because we have neglected the relatively small production outside of the $30-300$ eV energy interval. These radii would correspond to minimal pre-atmospheric weights of 220 kg for Abee and of 1.4 tons for Mezö-Madaras. The required mass for Abee seems not unreasonable, the recovered weight being 107 kg. From upper limits for neutron induced Cl^{36} activity in the same Abee sample BEGEMANN and VILCSEK [62] have derived an upper limit of 27 cm for the pre-atmospheric radius of Abee.

The recovered weight of Mezö-Madaras is only 23 kg. However, this meteorite fall is described by KNÖPFLER [63, 9] as follows: "After the appearance of a luminous meteor and detonations, a shower of many stones fell, of which the largest weighed about 10 kg". Thus, it may well be that Mezö-Madaras was a larger meteorite and that the main mass of the fall was never recovered. The observed Ne^{22}/Ne^{21} ratio would also be in agreement with a larger mass [13]. Mezö-Madaras is a relatively unaltered (primitive) meteorite [64] and its bromine and iodine content could be higher than the assumed average hypersthene chondrite values. Also the hydrogen content might be above average and thus the neutron moderation more effective. Both effects would considerably lower the required minimal mass.

For the Kr^{80} (n,γ) excesses in Bruderheim and H-Ausson, only upper limits of 1×10^{-12} cc STP/gm can be given. This seems somewhat astonishing because Bruderheim is a large meteorite. However, the Bruderheim sample of CLARKE and THODE [6] has a Xe^{128} excess of 8×10^{-12} cc STP/gm. The Kr isotopic composition is not known in their sample. It thus seems that our sample has either much lower Br and I contents or that it was located close to the pre-atmospheric surface of the meteorite.

There remains little doubt that the observed Kr^{80}, Kr^{82}, and Xe^{128} excesses in Abee are indeed due to cosmic ray produced neutrons. The same explanation for Mezö-Madaras would require that the meteorite was either much larger than indicated by the recovered mass or that it has above average H, Br, and I contents. Some evidence in favor for both requirements exists. At the present time it seems not necessary to invoke any "early irradiation" (neutral or charged) in order to explain the observed Kr^{80}, Kr^{82}, and I^{128} excesses.

Acknowledgements

We are very grateful to Prof. W. SCHOLLER, Vienna; Prof. R. E. FOLINSBEE, Edmonton and Dr. F. BEGEMANN, Mainz for providing us with meteorite samples. To Drs. H. DULAKAS and A. WYTTENBACH we are indebted for their unpublished results of Ca, Fe, Sr, and Ba determinations, to Dr. G. REED for unpublished Br and I concentrations, and to Dr. J. TRURAN for his unpublished cross section calculations. We would like to thank Drs. A. G. W. CAMERON, N. GRÖGLER, and F. G. HOUTERMANS for many stimulating discussions.

This work was supported by the Swiss National Science Foundation, Grants NF 2648, NF 3045, and NF 3468.

[62] F. BEGEMANN and E. VILCSEK, Z. Naturforschg. **20 a**, 533 [1965].

[63] W. KNÖPFLER, Verh. Siebenbürg. Ver. Naturwiss., Hermannstadt **4**, 19 [1853].

[64] J. A. WOOD, private communication 1964.

Rare Gas Measurements in 30 Stone Meteorites

P. EBERHARDT, O. EUGSTER, J. GEISS, and K. MARTI *

Physikalisches Institut, University of Berne, Switzerland

(Z. Naturforschg. **21 a**, 414—426 [1966]; received 30 November 1965)

The concentrations and isotopic composition of He, Ne and Ar in 29 chondrites and 1 achondrite have been determined. Detailed accounts of the experimental technique used and the reproducibility and accuracy obtained are given. The U,Th-He^4, and K-Ar ages derived from our results are in agreement with the already known age distributions of the different chondrite classes. Our measurements have revealed a linear correlation between the $(He^3/Ne^{21})_{spall}$ and the $(Ne^{22}/Ne^{21})_{spall}$ ratios, following the equation (constants for chondrites):

$$He^3/Ne^{21} = 2.40 + 23.4\,(Ne^{22}/Ne^{21} - 1)\ .$$

The significance of this correlation and its possible application in detecting diffusion losses are discussed. The radiation ages derived confirm the salient features observed in the radiation age distributions of the different chondrite classes. Five new meteorites with trapped gases were found (2 solar type, 3 planetary type).

1. General

During the last decade, the determination of the concentrations and isotopic compositions of rare gases in meteorites has become an important part of meteorite research and has given a great deal of information on the history of meteorites, the evolution of the solar system and on the intensity of cosmic radiation in the past. A considerable number of meteorites has been investigated and yet the accumulated body of data still seems to be insufficient to settle with statistical significance a number of important questions.

In this paper, we report and discuss concentrations and isotopic compositions of helium, neon and argon in 30 stone meteorites. In some of these meteorites, the isotopic abundances of krypton and xenon have also been determined [1].

It has been our aim in the present work to measure the three light rare gases with good relative and absolute accuracy in a restricted number of chondrites. The simultaneous determination of helium, neon and argon in the same sample is very important for the interpretation of the rare gas data. A high accuracy may reveal yet undiscovered correlations between different rare gas isotopes, radiation ages, radioactive ages, and other observational parameters. Very often results obtained in different laboratories have to be compared and thus a high absolute accuracy in the determination of isotopic compositions and concentrations is required.

Weathering and terrestrial temperatures may influence the rare gas content of a meteorite, and thus we have mainly investigated observed falls.

2. Meteorite Samples

The meteorite samples investigated were obtained from different collections and from some commercial sources. The relevant data on the meteorites (date of fall, recovered weight, fayalite content, classification, source of sample) are compiled in Table 1.

We were able to prove that two of our meteorite specimens are mislabelled. Magnetic measurements [8] showed that a meteorite specimen labelled Ausson and one labelled Mocs were both high iron chondrites. According to the classification in the literature [2, 3], however, both meteorites belong to the low iron class of chondrites. Such a variation of the chemical and mineralogical composition in one chondrite fall has never been observed yet and we must assume that some mislabelling has occurred.

We have a second specimen of Ausson indeed belonging to the low iron chondrite class. Its radiation age is lower by a factor of ten (to be publish-

* Present address: Department of Chemistry, University of California, La Jolla, Calif., U.S.A.

[1] K. MARTI, P. EBERHARDT, and J. GEISS, Z. Naturforschg. **21 a**, 398 [1966].

[2] G. T. PRIOR and M. H. HEY, Catalogue of Meteorites, British Museum, London 1953.

[3] B. MASON, Geochim. Cosmochim. Acta **27**, 1011 [1963].

Meteorite	Date of fall	Recovered weight kg	Fayalite content mol%	Classification	Source of sample
Atoka	9. 15. 1945	0.48	24	L	b
Baxter	1. 18. 1916	0.61	24	L	c
Benton	1. 16. 1949	5.4	31	LL	m
Bruderheim	3. 4. 1960	300	24	L	l
Calliham	found 1958	40	23	L	d
Colby (Wisconsin)	7. 4. 1917	105	25	L	c
Dhurmsala	7. 14. 1860	150	26	LL	e
Dimmitt	found	13.5	20	H	d
Finney	found	10.4	—	LL****	d
Harleton	5. 30. 1961	8.3	26	L	f
"H-Ausson"*	unknown	—	—	H	g
Kandahar (Afghanistan)	November 1959	0.68	24	L	h
Kesen	6. 12. 1850	135	17	H	c
Lanzenkirchen	8. 28. 1925	7	—	L	a
Marion, Kansas	found 1955	2.89	24	L	d
Maziba	9. 24 1942	5.0	25	L	b
Mezö-Madaras	9. 4. 1852	22.7	26	L	a
Mocs	2. 3. 1882	~300	24	L	i
Monte das Fortes	8. 23. 1950	4.9	24	L	j
Nerft	4. 12. 1864	10.25	23	L	a
Pribram	4. 7. 1959	9.5	20	H	k
"Pseudo-Pultusk"*	unknown	—	—	H	i
Saline	found***	31	18	H	c
St. Germain-du-Pinel	7. 4. 1890	~ 4	18	H	i
Shalka	11. 30. 1850	3.6**	—	D	a
Soko-Banja	10. 13. 1877	~80	27	LL	a
Tieschitz	7. 15. 1878	~28	—	L	a
Tysnes Island	5. 20. 1884	19.9	20	H	g
Waconda	found 1873	~50	25	L	a
Walters	7. 28. 1946	28	25	L	b

Table 1. Some relevant data on the investigated meteorites. Date of fall and recovered weight from PRIOR and HEY [2], MASON [3], KEIL [4], LEONARD [5]; fayalite content from MASON [3]. Classification: H=high iron chondrite; L=low iron chondrite; LL=amphoteric chondrite; D=diogenite (UREY and CRAIG [6], KEIL and FREDRIKSSON [7]). Sources of samples: [a] Prof. W. SCHOLLER, Naturhistorisches Museum, Wien; [b] Dr. E. P. HENDERSON, U.S. National Museum, Washington; [c] Prof. C. B. MOORE, Arizona State University, Tempe; [d] American Meteorite Laboratory, Denver; [e] Mineralien-Kontor Dr. F. KRANTZ, Bonn; [f] Prof. J. ARNOLD, University of California, San Diego; [g] Deyrolle, Paris; [h] Prof. M. GRÜNENFELDER, ETH, Zürich; [i] Mineralienhandlung Berger, Mödling; [j] Prof. A. DE CASTELLO BRANCO, Serviços Geologicos, Lisboa; [k] Prof. A. TUCEK, Narodni Museum, Praha; [l] Prof. R. E. FOLINSBEE, University of Alberta, Edmonton; [m] Proffs. R. DAVIES and O. SCHAEFFER, BNL, Brookhaven. * see text (chapter 2); ** probably much larger; *** possibly fell 11. 15. 1898; **** classification according to magnetic measurements (cf. EBERHARDT and GEISS [8]).

ed). The rare gas data of our high iron "Ausson" specimen are in good agreement with the results obtained by KIRSTEN, KRANKOWSKY, and ZÄHRINGER [9] on an alleged Ausson specimen. We thus conclude that the specimens measured by KIRSTEN et al. [9] and by us belong to the same, unknown high iron chondrite fall and we shall designate it as "H-Ausson".

The specimen labelled "Mocs" seems to belong to the Pultusk meteorite fall. The rare gas data are in fair agreement with results obtained on other specimens of Pultusk. Furthermore, meteorite specimens labelled Pultusk – obtained from the same commercial source as our alleged Mocs specimen – turned out to belong most likely to the Mocs meteorite fall [10]. It seems therefore that at

[4] K. KEIL, Fortschr. Mineral. **38**, 202 [1960].
[5] F. C. LEONARD, A Classificational Catalog of the Meteoritic Falls of the World, University of California press, Berkeley and Los Angeles 1956.
[6] H. C. UREY and H. CRAIG, Geochim. Cosmochim. Acta **4**, 36 [1953].
[7] K. KEIL and K. FREDRIKSSON, J. Geophys. Res. **69**, 3487 [1964].
[8] P. EBERHARDT and J. GEISS, in Isotopic and Cosmic Chemistry, dedicated to H. C. UREY (ed. H. CRAIG, S. L. MILLER, and G. J. WASSERBURG), North-Holland Publ. Co., Amsterdam 1964, p. 452.
[9] T. KIRSTEN, D. KRANKOWSKY, and J. ZÄHRINGER, Geochim. Cosmochim. Acta **27**, 13 [1963].
[10] H. HINTENBERGER, H. KÖNIG, L. SCHULTZ, and H. WÄNKE, Z. Naturforschg. **19 a**, 327 [1964], footnote 27.

some time specimens of Mocs and Pultusk have been confused and were subsequently sold with the wrong labelling. Therefore, we will designate our sample as "Pseudo-Pultusk".

3. Experimental Technique

3.1 Sample Preparation

For the analysis a piece of 2 to 5 gms of the meteorite specimen was chosen, if possible far away from any fusion crust. No samples were used which had been powdered previously. Any remaining fusion crust and surface contaminations were removed with a small dry abrasive wheel. A new wheel was used for each sample. The cleaned specimen was crushed on a stainless steel plate to a grain size finer than approximately 1 mm. Care was taken not to pulverize the sample too finely. Aliquots of 0.1 to 1 gram were then used for the individual rare gas determinations.

3.2 Rare Gas Extraction and Purification

Fig. 1 is a schematic drawing of the rare gas extraction and purification system used in this work. The meteorite samples were weighed into small Al-containers. Up to nine meteorite samples could be extracted without braking the vacuum. The whole extraction system was baked at 270 °C prior to extraction. The molybdenum crucible and the extraction jacket were thoroughly pre-degassed. The samples were heated to 70 °C for several hours to remove adsorbed atmospheric gases. The rare gases were extracted by melting the meteorite samples at 1700–1800 °C for 30 minutes. The evolved gases were purified in two steps with Ti-sponge and Ti-foil and subsequently Ar and He–Ne were transferred into separate sample tubes. Supremax glass sample tubes were used for the He–Ne fraction. All samples were subjected to an additional cleaning with hot Ti-foil, a hot CuO–Pd-mixture and hot CuO on the sample inlet system of the mass spectrometers.

In each set of samples at least one aliquot of the meteorites Dhurmsala or Kandahar was included. The completeness of the extraction was tested by at least one re-extraction at higher crucible temperature. The extraction blanks of our procedure were determined from extractions of empty aluminum containers, small meteorite samples of relatively low neon content, and from re-extractions. Blanks for He, Ne and Ar were 12, 0.2 and 0.5×10^{-8} cc STP respectively. For some samples measured early in this investigation, the neon and argon blanks were somewhat higher.

At least three extractions on aliquots of each meteorite sample were performed, two without spike for measuring the isotopic composition and one with a He^3–Ne^{22}–Ar^{38} spike for determining the concentrations by the isotopic dilution method. The sample sizes of the two extractions without spike were varied by about a factor of two. As a check, we have also calculated concentrations from ion beam intensities in all runs. The figures obtained in this way agree with the isotopic dilution results within 10%.

3.3 Mass Spectrometry

The rare gas samples were analyzed on all-glass, sector type, 60 degree, 10 cm radius of curvature, statically operated, UHV mass spectrometers with direct ion collection (without multiplier). No source magnet was employed for the helium and neon measurements. The sensitivity used was in the range of 2×10^{-6}, 4×10^{-6} and 3×10^{-5} amperes/cc STP for helium, neon and argon respectively. For most measurements, corrections due to machine background corresponded to less than 0.02×10^{-8} cc STP He^3 on mass 3 (HD), to less than 0.05×10^{-8} cc STP Ne^{20} on mass 20 (Ar^{++}) and to less than 0.1×10^{-8} cc STP Ne^{22} on mass 22 (CO_2^{++}). The mass spectrometer blank of atmospheric helium, neon and argon was always less than 10% of the extraction blank. Two spectrometers were employed in order to minimize the memory effect from the enriched gases used as spike. Mass discriminations in the spectrometer were always small (less than 1.5 percent per mass unit) and, furthermore, were always determined and corrected by measuring atmospheric argon and neon standards and a He^3/He^4 mixture prepared from calibrated amounts of pure He^3 and He^4. All our measurements are based on the ratios $Ar^{40}/Ar^{36} = 295.5$ (Nier [11]) and $Ne^{20}/Ne^{22} = 9.80$ (Eberhardt, Eugster, and Marti [12]) for atmospheric argon and neon.

3.4 Reproducibility and Accuracy

As mentioned above, a sample of a standard meteorite (Dhurmsala or Kandahar) was included in each set of meteorite samples. We have thus accumulated a considerable number of analyses of these two meteorites and the overall reproducibility of our whole measuring procedure can be calculated from these data. Tables 2 and 3 give the standard deviations for these repeated analyses, along with the average deviations observed between the duplicate analyses performed on all the other meteorites.

The observed standard deviations, and thus the errors for our experimental rare gas determination technique, are all smaller than 4% (except the Ar isotopes for Dhurmsala, see below). The Ne^{22}/Ne^{21} ratio has a standard deviation of less than one percent. The Ar^{40}/Ar^{36} and – to a lesser degree – the Ar^{40}/Ar^{38} ratios of Dhurmsala have a much higher standard deviation than those of Kandahar and of all the other samples. However, the Ar^{40}/Ar^{38}_{spall} ratio and also the absolute amount of Ar^{40} in Dhurmsala have standard deviations comparable to those obtained for the other meteorites. The large variations of Ar^{40}/Ar^{36}

[11] A. O. Nier, Phys. Rev. **77**, 789 [1950].

[12] P. Eberhardt, O. Eugster, and K. Marti, Z. Naturforschg. **20 a**, 623 [1965].

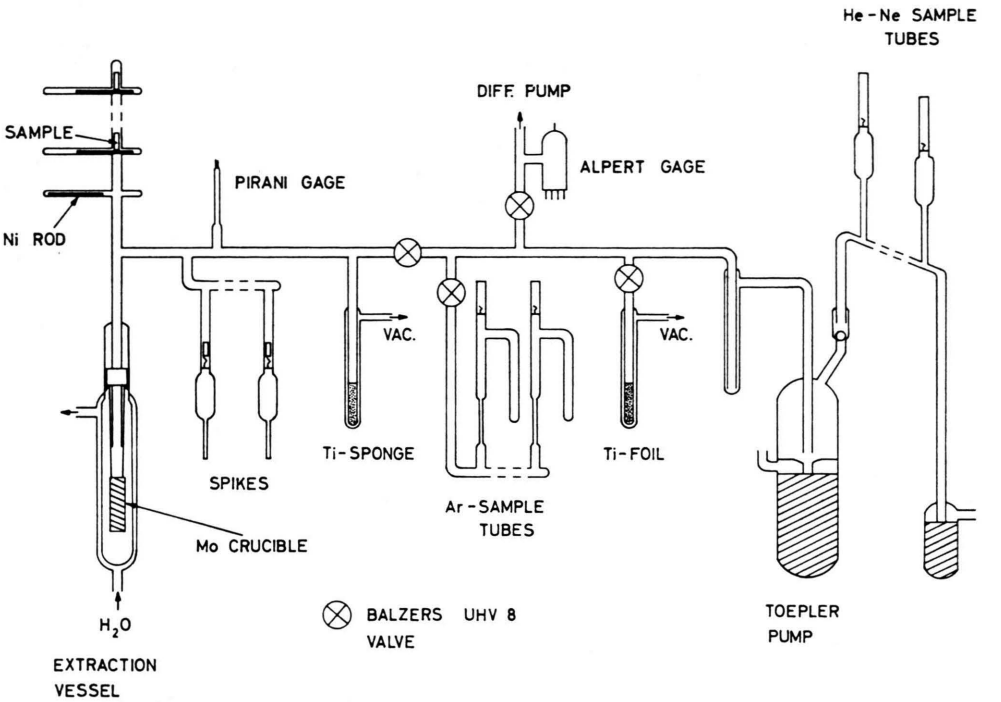

Fig. 1. Diagram of rare gas extraction and purification system used in this work.

meteorite	number of analyses	$\frac{He^3}{He^4}$	$\frac{Ne^{20}}{Ne^{21}}$	$\frac{Ne^{22}}{Ne^{21}}$	$\frac{Ar^{40}}{Ar^{36}}$	$\frac{Ar^{40}}{Ar^{38}}$	$\frac{Ar^{40}}{Ar^{38}_{spall}}$
Dhurmsala	12	1.8%	3.7%	0.8%	28 %*	11 %*	5.7%
Kandahar	9	2.7%	3.2%	0.8%	3.8%	3.5%	4.3%
Other samples		2.0%	4.0%	0.9%	2.4%	2.2%	3.3%

Table 2. Standard deviations of individual isotopic ratio measurements as derived from repeated analyses of aliquots of the Dhurmsala and Kandahar chondrites (sample sizes 0.3—0.7 gm). No measurements were discarded. Also given are the average deviations observed between the duplicate analyses of all the other meteorites. * The large variations in these isotopic ratios are presumably due to fluctuations in the trapped gas content (see text).

and Ar^{40}/Ar^{38} observed in different aliquots of Dhurmsala are thus probably due to fluctuations in the trapped gas content of this meteorite.

meteorite	number of analyses	He^4	Ne^{21}	Ar^{40}
Dhurmsala	4	0.6%	3.5%	1.5%
Kandahar	3	1.6%	1.2%	0.8%

Table 3. Standard deviations of individual isotopic concentration measurements by isotopic dilution as derived from repeated analyses of aliquots of the Dhurmsala and Kandahar chondrites (samples sizes 0.3—0.7 gm). No measurements were discarded.

Standards with known amounts of pure helium, neon and argon were prepared by filling calibrated sample tubes with a known gas pressure. Two independent methods were used for obtaining and measuring the pressure: (1) beginning with a high pressure measured with a mercury U-tube manometer, the gas was expanded into known volumes until the pressure was sufficiently low; (2) the filling pressure was directly measured with a McLeod gauge. The spikes were subsequently calibrated against these standards. The agreement finally obtained was better than 2%.

4. Results

The results of our rare gas measurements are compiled in Table 4. The chondrites are classified according to Urey and Craig [6] into high iron chondrites (H-chondrites), low iron chondrites (L-chondrites) and amphoteric chondrites (LL-chondrites [7]). Eberhardt and Geiss [8] have shown that such a classification is indeed justified for the discussion of the rare gas data of chondrites and that significant

Meteorite	He^3	He^4	Ne^{20}	Ne^{21}	Ne^{22}	Ar^{36}	Ar^{38}	Ar^{40}	$\frac{He^4}{He^3}$	$\frac{Ne^{20}}{Ne^{21}}$	$\frac{Ne^{22}}{Ne^{21}}$	$\frac{Ar^{40}}{Ar^{36}}$	$\frac{Ar^{36}}{Ar^{38}}$
L-Chondrites													
Atoka	7.6	570	1.11	1.23	1.38	0.83	0.33	6080	75.1	0.90	1.120	7350	2.5
	±0.4	±20	±0.09	±0.06	±0.08	±0.04	±0.05	±200	±2.0	±0.05	±0.030	±250	±0.4
Baxter	36.6	490	6.25	6.65	7.75	1.23	1.18	3380	13.4	0.94	1.165	2750	1.04
	±1.5	±13	±0.30	±0.25	±0.30	±0.05	±0.06	70	±0.3	±0.03	±0.015	± 90	±0.03
Bruderheim	52.4	561	8.8	9.90	10.9	1.56	1.56	1155	10.7	0.89	1.100	742	1.00
	±2.5	±20	±0.7	±0.50	±0.116	±0.09	±0.14	± 45	±0.3	±0.05	±0.020	± 20	±0.07
Calliham	44.6	321	8.8	9.70	10.6	1.49	1.16	330	7.2	0.91	1.090	222	1.28
	±3.0	± 9	±0.5	±0.35	±0.4	±0.06	±0.06	± 7	±0.4	±0.03	±0.010	± 7	±0.04
Colby,	45.0	563	9.7	10.6	11.5	1.89	1.50	2950	12.5	0.92	1.080	1560	1.26
Wisconsin	±2.0	±15	±0.5	±0.4	±0.5	±0.07	±0.07	± 60	± 0.3	±0.03	±0.010	± 50	±0.04
Harleton	70.4	602	11.7	12.7	14.2	2.15	1.92	970	8.55	0.92	1.120	450	1.12
	±3.0	±20	±0.8	±0.6	±0.8	±0.12	±0.14	± 35	±0.17	±0.04	±0.020	± 20	±0.05
Kandahar	40.5	1055	7.8	9.00	9.80	1.51	1.28	5790	26.1	0.87	1.090	3840	1.18
	±1.2	±20	±0.3	±0.25	±0.30	±0.04	±0.04	± 90	±0.4	±0.02	±0.010	± 80	±0.02
Lanzen-	66.8	488	14.5	15.9	17.6	3.12	2.48	1285	7.3	0.92	1.105	415	1.26
kirchen	±3.5	±13	±0.7	±0.6	±0.7	±0.35	±0.30	± 25	±0.3	±0.03	±0.010	± 30	±0.04
Marion,	64.0	1505	12.3	13.4	14.8	7.40	2.60	7760	23.5	0.92	1.105	1050	2.84
Kansas	±2.5	±40	±0.6	±0.5	±0.6	±0.40	±0.18	±150	±0.5	±0.03	±0.010	± 50	±0.12
Maziba	46.9	1225	5.7	6.25	7.55	1.25	1.10	5900	26.1	0.91	1.210	4720	1.14
	±2.0	±45	±0.4	±0.30	±0.45	±0.06	±0.07	±200	±0.6	±0.04	±0.020	±150	±0.09
Mezö-	51.3	836	11.8	11.1	12.5	52.2	11.3	1255	16.3	1.06	1.125	24.0	4.61
Madaras	±2.5	±25	±0.6	±0.4	±0.5	±2.5	±0.6	± 25	±0.5	±0.04	±0.010	± 1.0	±0.10
Mocs	24.5	707	5.5	6.65	7.00	1.31	0.92	5630	28.1	0.83	1.055	4300	1.43
	±1.0	±18	±0.5	±0.25	±0.25	±0.06	±0.05	±120	±0.6	±0.06	±0.010	±170	±0.04
Monte das	51.2	1425	10.7	11.6	12.8	1.92	1.59	5620	27.8	0.92	1.100	2920	1.21
Fortes	±2.0	±40	±0.6	±0.4	±0.5	±0.20	±0.20	±120	±0.6	±0.03	±0.010	±300	±0.10
Nerft	63.5	470	12.0	13.0	14.0	2.02	1.98	270	7.4	0.92	1.080	133.2	1.02
	±2.5	±12	±0.6	±0.5	±0.5	±0.08	±0.10	± 6	±0.2	±0.03	±0.010	± 4.0	±0.03
Tieschitz	45.8	1685	9.0	7.50	9.15	22.8	5.34	2280	36.8	1.20	1.220	100	4.27
	±1.5	±45	±0.5	±0.25	±0.35	±0.9	±0.25	± 50	±0.7	±0.05	±0.010	± 3	±0.10
Waconda	24.7	1305	5.5	5.90	6.43	1.24	0.92	5620	52.9	0.93	1.090	4530	1.35
	±1.0	±35	±0.3	±0.20	±0.25	±0.05	±0.05	±120	±1.1	±0.03	±0.010	±150	±0.04
Walters	4.4	331	1.16	1.27	1.33	0.98	0.33	2140	74.7	0.91	1.050	2180	2.94
	±0.2	±15	±0.09	±0.06	±0.08	±0.05	±0.04	± 70	±2.5	±0.05	±0.030	± 70	±0.30
H-Chondrites													
Dimmitt	3.8	4030	58.2	1.83	6.74	7.50	1.58	1950	1075	31.8	3.68	259	4.76
	±0.2	±100	±3.0	±0.07	±0.30	±0.30	±0.07	± 40	±30	±1.0	±0.07	± 8	±0.12
"H-Ausson"	101	1610	19.5	21.7	23.9	3.53	3.36	6110	15.9	0.90	1.100	1730	1.05
	±4	±40	±1.0	±0.8	±0.9	±0.13	±0.17	±130	± 0.3	±0.03	±0.010	± 50	±0.03
Kesen	12.2	1455	1.90	2.62	2.82	1.95	0.67	5300	119	0.72	1.075	2720	2.89
	±0.5	±40	±0.28	±0.09	±0.11	±0.07	±0.03	±110	± 3	±0.10	±0.020	± 90	±0.09
"Pseudo-	8.9	5690	16.2	2.02	3.35	2.35	0.65	5710	639	8.0	1.66	2430	3.59
Pultusk"	±0.4	±150	±0.9	±0.07	±0.15	±0.09	±0.03	±120	±15	±0.3	±0.03	± 80	±0.10
Pribram	23.9	1315	5.0	5.10	5.56	1.10	0.77	4170	55.0	0.98	1.090	3800	1.43
	±1.2	± 50	±0.4	±0.25	±0.30	±0.06	±0.09	±140	± 1.6	±0.04	±0.020	±120	±0.14

Table 4

Meteorite	He^3	He^4	Ne^{20}	Ne^{21}	Ne^{22}	Ar^{36}	Ar^{38}	Ar^{40}	$\frac{He^4}{He^3}$	$\frac{Ne^{20}}{Ne^{21}}$	$\frac{Ne^{22}}{Ne^{21}}$	$\frac{Ar^{40}}{Ar^{36}}$	$\frac{Ar^{36}}{Ar^{38}}$
Saline	9.4	1245	1.56	1.79	2.01	1.91	0.64	4390	132	0.87	1.125	2290	3.00
	±0.4	±35	±0.09	±0.07	±0.08	±0.07	±0.03	±90	±3	±0.04	±0.015	±70	±0.10
St. Germain-du-Pinel	9.5	1260	2.08	2.54	2.69	1.46	0.59	5150	132	0.82	1.060	3520	2.48
	±0.4	±35	±0.15	±0.09	±0.11	±0.06	±0.03	±110	±4	±0.05	±0.015	±110	±0.07
Tysnes Island	38.4	109000	415	3.22	38.6	25.5	5.25	4820	2840	129	12.0	189	4.86
	±1.5	±3000	±25	±0.15	±2.0	±2.7	±0.60	±100	±70	±3	±0.2	±18	±0.15
LL-Chondrites													
Benton	47.5	1335	8.6	9.75	10.7	1.18	1.37	5370	28.1	0.88	1.100	4540	0.86
	±2.0	±35	±0.45	±0.35	±0.4	±0.05	±0.07	±110	±0.6	±0.03	±0.010	±140	±0.02
Dhurmsala	14.0	529	3.77	4.05	4.35	1.16	0.64	3410	37.8	0.93	1.075	2940	1.80
	±0.4	±11	±0.13	±0.12	±0.14	±0.12	±0.08	±60	±0.5	±0.02	±0.010	±300	±0.10
Finney	29.4	708	3.80	3.92	4.65	1.13	0.68	4100	24.1	0.97	1.185	3620	1.67
	±1.2	±18	±0.20	±0.14	±0.17	±0.04	±0.03	±90	±0.6	±0.03	±0.010	±110	±0.05
Soko Banja	110	1750	24.3	26.7	29.5	6.78	4.16	9490	15.9	0.91	1.105	1400	1.63
	±4	±45	±1.2	±0.9	±1.1	±0.25	±0.20	±200	±0.4	±0.03	±0.010	±50	±0.05
Diogenite													
Shalka	39.4	209	5.9	6.20	7.20	0.57	0.28	120	5.3	0.94	1.160	211	2.0
	±2.0	±4	±0.3	±0.20	±0.30	±0.12	±0.13	±5	±0.2	±0.03	±0.020	±40	±0.8

Table 4. Results of rare gas analyses. All concentrations in units of 10^{-8} cc STP/gm.

differences exist between the age distributions of L- and H-chondrites.

The reproducibility of our experimental procedure, as determined from the repeated analyses of Dhurmsala and Kandahar (see 3.4), has served as basis for the assignment of errors. Additional factors, such as sample size or absolute rare gas concentration, were also taken into account. The absolute error of our gas standards used for spike calibrations is included in the errors given for the concentrations.

With a few exceptions, we had chosen meteorites for which no or only incomplete rare gas data were available in the literature at the time of measurement. In the meantime, however, rare gas results have been published of an additional number of meteorites included in our investigation. A comparison between our results and those published by other investigators is hampered by the following two factors:

a) The meteorite samples used are not aliquots and thus some variations in the rare gas contents between different samples cannot be excluded. However, the uranium, thorium and potassium contents in ordinary chondrites are fairly constant [9, 13–20], and thus radiogenic He^4 and Ar^{40} are not expected to vary for different samples of the same meteorite, provided each sample represents a good average. If very small samples are used, variations may be introduced by mineralogical and chemical inhomogeneities. Large variations in the trapped gas content in the same meteorite do occur, and therefore no comparison of this gas component is possible. Of course, also the possibility exists that meteorite samples are mislabelled.

b) No individual errors are assigned to most of the published data.

The average relative deviations $|\bar{\delta}|$ and the mean of the relative deviations $\bar{\delta}$ observed between the

[13] H. Hamaguchi, G. W. Reed, and A. Turkevich, Geochim. Cosmochim. Acta **12**, 337 [1957].
[14] G. L. Bate, J. R. Huizenga, and H. A. Potratz, Geochim. Cosmochim. Acta **16**, 88 [1959].
[15] H. König and H. Wänke, Z. Naturforschg. **14 a**, 866 [1959].
[16] G. W. Reed, K. Kigoshi, and A. Turkevich, Geochim. Cosmochim. Acta **20**, 122 [1960].
[17] G. G. Goles and E. Anders, Geochim. Cosmochim. Acta **26**, 723 [1962].
[18] G. Edwards and H. C. Urey, Geochim. Cosmochim. Acta **7**, 154 [1955].
[19] G. Edwards, Geochim. Cosmochim. Acta **8**, 285 [1955].
[20] J. Geiss and D. C. Hess, Astrophys. J. **127**, 224 [1958].

published and our results are given in Table 5. The average relative deviations are two to eight times larger than the accuracy of our own results. The best agreement is obtained for the Ne^{22}/Ne^{21} ratio. This is not surprising because this ratio varies by only 20% between different meteorites, whereas all the other ratios are much less constant. The mean of the relative deviations is, with the exception of the Ne^{20}/Ne^{21} ratio, always much smaller than the average deviation. Thus, no large systematic differences between our results and the published data seem to occur. The discrepancy in the Ne^{20}/Ne^{21} ratio may be due to an underestimation of the Ne^{20} blank correction in many of the literature data, and to the use of the old value $Ne^{20}/Ne^{22} = 10.3$ for terrestrial neon. This should also lead to systematic differences in the Ne^{22}/Ne^{21} values.

It is important to consider these random differences which seem to exist between rare gas measurements performed by different laboratories, if conclusions are based on results from many investigators. As an illustration, let us consider a set of meteorites created in one break-up process. They will have exactly the same radiation age. If these meteorites were measured by different laboratories, a minimum line width of 20% for the radiation age distribution would result from the experimental errors. If the radiation ages are derived from the concentration of He^3 alone, an additional line broadening by approximately 30% would occur, due to variations in shielding. Thus, the measuring and evaluation technique used transforms this initial δ-function into a broad peak with a line width of approximately 40%. If Ne^{21} is used instead of He^3 the resulting line broadening would be even larger (cf. chapter 6.2). Thus, individual events in the history of meteorite parent bodies will be masked if they occur too frequently.

5. Radiogenic Ages

The potassium content of most L- and H-chondrites is constant within $\pm 10\%$ [9, 18–20] and also uranium and thorium do not show large variations [13–17]. It is therefore possible to calculate K^{40}-Ar^{40} and U, Th-He^4 ages from the rare gas data alone (Table 6). Average uranium, thorium and potassium contents of 0.012, 0.043 and 850 ppm respectively were used for L- and H-chondrites. He^4 was corrected for the contribution from spallation assuming $He^4/He^3 = 4$ in spallation produced helium [9]. This correction is small except for some meteorites with U,Th-He^4 ages below 10^9 years. The following decay constants were used for the calculation of the ages:

$$\lambda(U^{238}) = 1.54 \times 10^{-10} \text{ yrs}^{-1};$$
$$\lambda(U^{235}) = 9.8 \times 10^{-10} \text{ yrs}^{-1};$$
$$\lambda(Th^{232}) = 4.99 \times 10^{-11} \text{ yrs}^{-1};$$
$$\lambda_{tot}(K^{40}) = 5.46 \times 10^{-10} \text{ yrs}^{-1};$$
$$\lambda_k(K^{40}) = 6.02 \times 10^{-11} \text{ yrs}^{-1}.$$

The potassium content of LL-chondrites is not as constant as in L- and H-chondrites (KAISER and ZÄHRINGER [21]). Thus, no radiogenic ages are given for this chondrite class.

The U,Th-He^4 and K-Ar^{40} ages obtained for the investigated chondrites show the general behavior characteristic for chondrites:

1. Most K-Ar^{40} ages of chondrites lie between 3.5 and 4.6×10^9 years (GEISS and HESS [20]; KIRSTEN, KRANKOWSKY, and ZÄHRINGER [9]).

	He^3	He^4	Ne^{20}	Ne^{21}	Ne^{22}	Ar^{36}	Ar^{38}	Ar^{40}	$\frac{He^4}{He^3}$	$\frac{Ne^{20}}{Ne^{21}}$	$\frac{Ne^{22}}{Ne^{21}}$	$\frac{Ar^{40}}{Ar^{36}}$	$\frac{Ar^{36}}{Ar^{38}}$
Average relative deviation $\overline{\lvert\delta\rvert}$	8%	14%	11%	10%	12%	16%	17%	9%	12%	9%	4%	12%	10%
Mean of relative deviations $\bar{\delta}$	+4%	−1%	+4%	−3%	−6%	−9%	−8%	−5%	+6%	+8%	−2%	−6%	+1%
Number of comparisons	24	22	18	21	20	10	11	12	21	17	20	10	11

Table 5. Average relative deviations $\overline{|\delta|} = \frac{1}{n} \sum \left| \left(\frac{x_i}{x_0} - 1 \right) \right|$ and mean of relative deviations $\bar{\delta} = \frac{1}{n} \sum \left(\frac{x_i}{x_0} - 1 \right)$ observed between our results and those of other workers. x_0: our measurements, x_i: published measurements. Values deviating by more than 50% from our own results have been discarded, as well as those meteorites containing trapped gases. $\bar{\delta}$ is a measure for systematic differences between the published and our results, $\overline{|\delta|}$ indicates random fluctuations.

[21] W. KAISER and J. ZÄHRINGER, Z. Naturforschg. **20 a**, 963 [1965].

Sample	He^3_{spall}	Ne^{21}_{spall}	Ar^{38}_{spall}	$\frac{He^3_{spall}}{Ne^{21}_{spall}}$	$\frac{Ne^{22}_{spall}}{Ne^{21}_{spall}}$	He^3-age	U,Th-He^4 age	K-Ar-age
	10^{-8} cc STP/gm					10^6 years		
L-Chondrites								
Atoka	7.6	1.23	0.21	6.18	1.120	3.8	1800	4440
Baxter	36.5	6.65	1.08	5.49	1.160	18.2	1200	3470
Bruderheim	52.4	9.9	1.44	5.29	1.100	26.2	1200	1950
Calliham	44.6	9.7	1.00	4.60	1.090	22.3	520	780
Colby, Wisconsin	45.0	10.6	1.31	4.25	1.080	22.5	1300	3250
Harleton	70.4	12.7	1.73	5.54	1.12	35.2	1100	1730
Kandahar	40.5	9.0	1.14	4.50	1.090	20.2	2700	4350
Lanzenkirchen	66.8	15.9	2.16	4.20	1.105	33.4	780	2080
Marion, Kansas	64.0	13.4	1.39	4.78	1.105	32.0	3450	4860
Maziba	46.9	6.25	0.99	7.50	1.210	23.4	3000	4390
Mezö-Madaras	51.3	11.1	—	4.62	1.110	25.6	2050	2050
Mocs	24.5	6.65	0.77	3.68	1.060	12.2	1950	4310
Monte das Fortes	51.2	11.6	1.40	4.41	1.100	25.6	3400	4300
Nerft	63.5	13.0	1.82	4.88	1.080	31.8	760	660
Tieschitz	45.8	7.5	—	6.11	1.195	22.9	—	2860
Waconda	24.7	5.9	0.78	4.19	1.085	12.4	3350	4300
Walters	4.4	1.27	0.17	3.46	1.050	2.2	1100	2770
H-Chondrites								
Dimmitt	3	1.67	—	—	—	1.5	—	2640
"H-Ausson"	101	21.7	3.1	4.65	1.100	50.5	3350	4440
Kesen	12.2	2.62	0.35	4.66	1.090	6.1	3700	4200
"Pseudo-Pultusk"	7.7	1.98	0.24	—	—	3.8	—	4330
Pribram	23.9	5.1	0.64	4.69	1.085	12.0	3400	3810
Saline	9.4	1.79	0.32	5.25	1.125	4.7	3350	3890
St. Germain-du-Pinel	9.5	2.54	0.36	3.74	1.065	4.8	3400	4150
Tysnes Island	—	2.0	—	—	—	(4)	—	4040
LL-Chondrites								
Benton	47.5	9.75	1.31	4.87	1.100	23.8	—	—
Dhurmsala	14.0	4.05	0.48	3.46	1.070	7.0	—	—
Finney	29.4	3.92	0.53	7.50	1.180	14.7	—	—
Soko Banja	110	26.7	3.3	4.12	1.105	55	—	—
Diogenite								
Shalka	39.4	6.20	0.20	6.35	1.155	—	—	—

Table 6. Concentrations and ratios of spallation produced isotopes, radiation ages and radiogenic ages of investigated meteorites.

2. U,Th-He^4 ages are either concordant or lower than K-Ar^{40} ages, in the latter case indicating diffusion loss (EBERHARDT and HESS [22]; ANDERS [23]).
3. The age distribution of L- and H-chondrites is different, implying different histories (EBERHARDT and GEISS [8]; KEIL [24]; ANDERS [25]).

All these features can be easily deduced from a histogram of the K-Ar^{40} ages, as given in Fig. 2. In addition to our results also all other known chondrite ages have been plotted (cf. ZÄHRINGER [26]). However, only meteorites with concordant He^4 and Ar^{40} ages have been included. We define these two ages as concordant, if the He^4 age does not deviate by more than 25% from the Ar^{40} age. This rather generous definition of concordance has to be used because of the uncertainty in the uranium, thorium and potassium contents, and also in view of the experimental errors of the rare gas concentrations. Concordant ages are much more frequent for the H-chondrites than for the L-chondrites [26] (75% against 42%). Several explanations for this systematic difference between the two chondrite classes seem possible: (1) The minerals in L-chondrites have larger diffusion coefficients for rare gases than those in H-chondrites. (2) The grain size distributions are different. (3) The temperature in L-chondrites was on the average higher than that in H-chondrites. (4) The L-chondrites have been reheated at some time in their history, resulting in

[22] P. EBERHARDT and D. C. HESS, Astrophys. J. **131**, 38 [1960].
[23] E. ANDERS, Rev. Mod. Phys. **34**, 287 [1962].
[24] K. KEIL, Nature **203**, 511 [1964].
[25] E. ANDERS, Space Sci. Rev. **3**, 583 [1964].
[26] J. ZÄHRINGER, Chronology of Chondrites with Rare Gas Isotopes, preprint [1965].

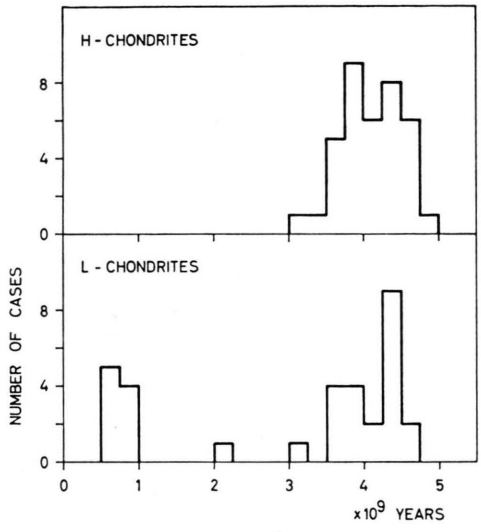

Fig. 2. Histogram of K/Ar^{40} ages. Only meteorites with concordant ages (He^4 age within $\pm 25\%$ of the $K\text{-}Ar^{40}$ age) are included. Ages from this paper and from summary in ZÄHRINGER's [26] publication.

total or partial loss of the rare gases. The occurrence of a sizable number of L-chondrites with concordant ages of around 600 m.y. makes the last of the four explanations the most likely one (ANDERS [25]).

6. Spallation Produced Isotopes

In Table 6 the concentrations of spallation produced He^3, Ne^{21}, and Ar^{38} of the investigated meteorites are listed. A correction for trapped gases (primordial gases) was applied, using the ratios $He^4/He^3 = 3500$; $Ne^{20}/Ne^{21} = 340$; $Ne^{20}/Ne^{22} = 11.4$ and $Ar^{36}/Ar^{38} = 5.35$ in the trapped component; $Ne^{20}/Ne^{21} = 0.9$ and $Ar^{36}/Ar^{38} = 0.65$ in the spallation component. Ar^{40} was not corrected.

With the exception of the three gas-rich meteorites, Tysnes Island, "Pseudo-Pultusk" and Dimmitt, the corrections for He^3 and Ne^{21} were less than 0.1% and for Ne^{22} less than 2%. Thus, they cannot introduce an appreciable error, even if the above assumed isotopic compositions of the trapped component should show some variations from one meteorite to the other. In most cases the correction for trapped Ar^{38} was less than 40%.

6.1 Correlation Between Spallation Produced Isotopes

It has been recognized for some time that certain correlations exist between spallation produced isotopes in iron meteorites [27, 28]. These correlations are in agreement with general spallation theory [29, 30]. From the abundance ratio of spallation produced isotopes such as Ar^{38} and Ne^{21} the hardness of the irradiation spectrum in the meteorite sample itself can be calculated [29], and thus the amount of shielding and the pre-atmospheric mass of an iron meteorite can be estimated [31].

The first measurements of rare gases in stone meteorites showed that in most chondritic meteorites the ratio of spallation produced isotopes are fairly constant. Large variations did, of course, occur between chondrites and the different classes of achondrites [20, 22, 32–34]. In the last few years, it was then recognized that the He^3/Ne^{21} ratio in chondrites is not constant and in extreme cases variations by a factor of three or more have been observed [9, 35]. As this effect could not be explained by differences in chemical composition, it was thought that it is due to variations in shielding [9] and to preferential diffusion loss of He^3.

HINTENBERGER, VILCSEK, and WÄNKE [36] have shown that certain minerals in the chondrite Breitscheid have indeed lost He^3, indicating that diffusion has affected the He^3/Ne^{21} ratio of 3.8. It is reported [37] that the low He^3/Ne^{21} ratios of 1.42 and 0.67 for Cullison and Seres respectively are also due to diffusion.

However, Parnallee with $He^3/Ne^{21} = 2.73$ does not seem to have suffered diffusion losses [37]. Thus, the observed variations in the He^3/Ne^{21} ratio cannot be explained by diffusion loss alone.

[27] K. H. EBERT and H. WÄNKE, Z. Naturforschg. **12a**, 766 [1957].
[28] P. SIGNER and A. O. NIER, J. Geophys. Res. **65**, 2947 [1960].
[29] J. GEISS, H. OESCHGER, and U. SCHWARZ, Space Sci. Rev. **1**, 197 [1962].
[30] J. R. ARNOLD, M. HONDA, and D. LAL, J. Geophys. Res. **66**, 3519 [1961].
[31] P. SIGNER and A. O. NIER, in Researches in Meteorites (ed. C. B. MOORE), John Wiley & Sons, New York 1962.
[32] A. EBERHARDT and P. EBERHARDT, Helv. Phys. Acta **33**, 593 [1960] and Z. Naturforschg. **16a**, 236 [1961].
[33] H. STAUFFER, J. Geophys. Res. **66**, 1513 [1961].
[34] H. STAUFFER, J. Geophys. Res. **67**, 2023 [1962].
[35] H. HINTENBERGER, H. KÖNIG, L. SCHULTZ, and H. WÄNKE, Z. Naturforschg. **19a**, 327 [1964].
[36] H. HINTENBERGER, E. VILCSEK, and H. WÄNKE, Z. Naturforschg. **19a**, 219 [1964].
[37] H. HINTENBERGER, H. KÖNIG, L. SCHULTZ, and H. WÄNKE, Z. Naturforschg. **20a**, 983 [1965].

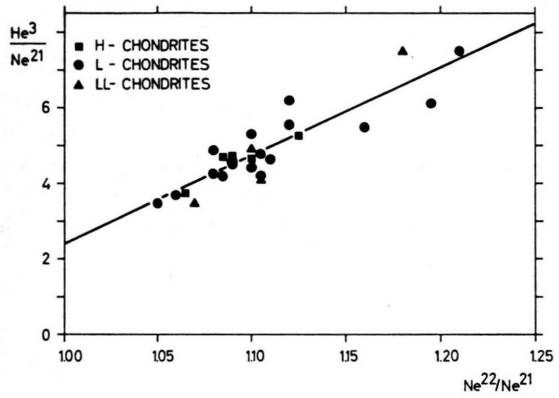

Fig. 3. $(He^3/Ne^{21})_{spall}$ versus $(Ne^{22}/Ne^{21})_{spall}$ diagram for chondrites. Data from this paper only. The correlation line has been calculated by the least square method.

From our results, as given in Table 6, we have found that a strong correlation exists between the $(He^3/Ne^{21})_{spall}$ and $(Ne^{22}/Ne^{21})_{spall}$ ratios. Fig. 3 shows this correlation in a $He^3/Ne^{21} - Ne^{22}/Ne^{21}$ diagram. Only our measurements have been included. The correlation seems to be linear within the errors of our measurements and the straight line drawn in Fig. 3 has been calculated by the least square method. It is represented by the equation

$$He^3/Ne^{21} = C + m\left(\frac{Ne^{22}}{Ne^{21}} - 1\right) \qquad (1)$$

with $C = 2.40$ and $m = 23.4$.

Among the published rare gas data on chondrites, only those of KIRSTEN, KRANKOWSKY, and ZÄHRINGER [9] show this correlation, but with a somewhat larger scatter than our measurements. The correlation is not clearly visible in the results of other authors, except for meteorites with extreme He^3/Ne^{21} ratios.

Three parameters can influence the position of a meteorite in the $He^3/Ne^{21} - Ne^{22}/Ne^{21}$ diagram: a) chemical composition; b) cosmic ray energy spectrum; c) diffusion loss.

6.1.1 Chemical Composition

In stone meteorites the neon isotopes are produced almost exclusively from spallation reactions on the elements sodium to sulphur. In chondrites magnesium alone contributes about 2/3 of the total production, and silicon a large fraction of the remainder [34, 38]. The He^3 production rate is similar for all elements.

The average MgO content of the three classes of chondrites differs slightly. L-chondrites contain on the average 6% and LL-chondrites 8% more MgO than H-chondrites [6, 39]. The average variation of the MgO content within one of these chondritic classes is about ±2% (CRAIG [39]). The variations of SiO_2 go roughly parallel with those of MgO, and therefore the ratio MgO/SiO_2 is quite constant. Thus, differences in the chemical composition between the chondrites will not influence the Ne^{22}/Ne^{21} ratio and can only lead to variations of ±5% in the He^3/Ne^{21} ratio.

The systematic differences in the MgO contents between the three chondrite classes should result in slightly different correlation lines. The slope m and the constant C in Eq. (1) should differ by approximately 6% between H and L and by 8% between H- and LL-chondrites. However, with the present-day accuracy and the rather limited number of measurements, these differences are masked by experimental error, and it is justified to treat all chondrites as one class.

6.1.2 Cosmic Ray Energy and Composition Spectrum

The production ratio of two spallation isotopes depends on the energy and composition spectrum of the radiation in the sample. The correlation found between He^3/Ne^{21} and Ne^{22}/Ne^{21} suggests that mainly variations in the neon production rate are the source for the observed variations in the He^3/Ne^{21} ratio. From tritium measurements it is known that the He^3 production rate in most chondrites is indeed constant within ±20% [40, 41]. The cross section for Ne^{21} production from Mg, Al and Si is roughly constant for protons with energies between 0.6 and 24 GeV, whereas the He^3 production cross section seems to be somewhat more energy dependent [9, 42]. Charged particles with energies below a few hundred MeV contribute relatively little to the production of

[38] H. HINTENBERGER, H. KÖNIG, L. SCHULTZ, H. WÄNKE, and F. WLOTZKA, Z. Naturforschg. **19 a**, 88 [1964].

[39] H. CRAIG, in Isotopic and Cosmic Chemistry, dedicated to H. C. UREY (ed. H. CRAIG, S. MILLER, and G. WASSERBURG), North-Holland Publ. Co., Amsterdam 1964.

[40] J. GEISS, H. OESCHGER, and P. SIGNER, Z. Naturforschg. **15 a**, 1116 [1960].

[41] K. GOEBEL and P. SCHMIDLIN, Z. Naturforschg. **15 a**, 79 [1960].

[42] K. GOEBEL, H. SCHULTES, and J. ZÄHRINGER, CERN-report CERN 64-12 [1964].

spallation isotopes. Secondary neutrons in this energy range will, however, make an appreciable contribution to the total production, because they are not slowed down by ionization. After cosmic radiation has passed through one interaction length, the number of neutrons should be equal to or larger than the number of protons. Neutrons with energies between ten and a few hundred MeV will, to a large extent, induce spallation reactions resulting in small ΔA, such as

$$Mg^{24}(n,2pn)Ne^{22}, \quad Mg^{24}(n,p2n)Na^{22}(\beta)Ne^{22},$$
$$Mg^{24}(n,\alpha)Ne^{21}.$$

Thus, in large stone meteorites secondary neutrons will make an appreciable contribution to the total neon production [33].

If this explanation holds, high He^3/Ne^{21} ratios should be found only in small meteorites. A comparison of Tables 1 and 6 and a survey of the literature shows that all meteorites with $Ne^{22}/Ne^{21} > 1.15$ are small, the recovered weights corresponding to radii of less than 15 cm.

The He^3/Ne^{21} production ratio in chondrites of the primary cosmic radiation must thus be equal to or higher than 7, the highest value observed. Such a ratio corresponds to an average energy of 600 MeV (cf. Fig. 4 in KIRSTEN, KRANKOWSKY, and ZÄHRINGER [9]).

In chondrites, Ar^{38} is produced in approximately equal amounts from calcium and iron. The production of Ar^{38} from Ca^{40} is similar to the production of Ne^{22} from Mg^{24}, i. e. mass loss $\Delta A = 2$ and heavy contribution by secondary neutrons in both cases. Therefore, it is to be expected that the Ne^{22}/Ar^{38} ratio is more constant than the He^3/Ar^{38} ratio. A comparison of meteorites with extreme He^3/Ne^{21} values shows that this is indeed true. The L-chondrites Walters, Bruderheim, and Maziba have constant Ne^{22}/Ar^{38} ratios of 7.8, 7.6 and 7.6, whereas the He^3/Ar^{38} ratios are 26, 36 and 47. The LL-chondrites Dhurmsala and Finney have Ne^{22}/Ar^{38} ratios of 9.0 and 8.7 and He^3/Ar^{38} ratios of 29 and 55. The average Ne^{22}/Ar^{38} ratios of H-, L- and LL-chondrites are 7.6, 8.2 and 8.7 respectively. The variations are, of course, due to the systematic differences in the iron contents of the three classes.

6.1.3. Diffusion Loss

Partial diffusion loss will mainly affect He^3/Ne^{21}. No great change is to be expected in the Ne^{22}/Ne^{21} ratio (preferential diffusion loss in certain minerals may result in small changes). Thus, diffusion loss will move a meteorite in the $He^3/Ne^{21} - Ne^{22}/Ne^{21}$ diagram parallel or nearly parallel to the ordinate in the direction of smaller He^3/Ne^{21} values.

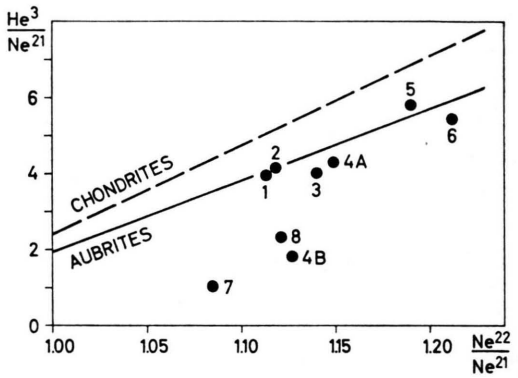

Fig. 4. $(He^3/Ne^{21})_{spall}$ versus $(Ne^{22}/Ne^{21})_{spall}$ correlation diagram for aubrites. The aubritic correlation line is not fitted but has been calculated from the one for chondrites. (1) Norton County, (2) Khor Temiki, (3) Bustee, (4A) and (4B) two Bishopville samples, (5) Shallowater, (6) Peña Blanca Spring, (7) Cumberland Falls, (8) Aubres.

As an illustration, we will discuss the case of the enstatite achondrites (aubrites). Figure 4 is a $He^3/Ne^{21} - Ne^{22}/Ne^{21}$ diagram for the aubrites. The data used are from EBERHARDT, EUGSTER, and GEISS [43] and KIRSTEN, KRANKOWSKY, and ZÄHRINGER [9]. The Ne^{22}/Ne^{21} ratios of the latter authors have been recalculated for $Ne^{20}/Ne^{22} = 9.80$ in the terrestrial atmosphere. The He^3 production rate in aubrites is 1.11 and the Ne^{21} production rate is 1.38 times higher than in chondrites [43]. For the same irradiation spectrum, He^3/Ne^{21} ratios are thus 20% smaller in aubrites than in chondrites. The Ne^{22}/Ne^{21} ratio is not affected because the Mg/Si ratios in aubrites and chondrites are virtually equal. The correlation line for aubrites, shown in Fig. 4, has been calculated from the correlation line for chondrites with

$$C(\text{aubrites}) = \tfrac{1.11}{1.38} \times C(\text{chondrites}),$$
$$m(\text{aubrites}) = \tfrac{1.11}{1.38} \times m(\text{chondrites}).$$

Six aubrites (Shallowater, one sample of Bishopville, Norton County, Khor Temiki, Bustee, Peña Blanca Spring) lie

[43] P. EBERHARDT, O. EUGSTER, and J. GEISS, J. Geophys. Res. **70**, 4427 [1965].

within $\pm 12\%$ of the correlation line. Cumberland Falls, Aubres and a second sample of Bishopville, however, have much lower He^3/Ne^{21} ratios than would correspond to their Ne^{22}/Ne^{21} values. These three meteorites must have suffered considerable He^3 diffusion losses. The difference in the Ne^{21} content of the two Bishopville samples is only 10%, whereas the He^3 differs by more than a factor of two. The Ne^{22}/Ne^{21} ratio in both Bishopville samples is the same within the limits of experimental error. From the Ne^{22}/Ne^{21} ratios, we deduce that the He^3/Ne^{21} production ratio was 3.5 in Cumberland Falls and 4.0 in Aubres.

From the foregoing discussion it is evident that the He^3/Ne^{21} ratio alone is not necessarily a good criterion for diffusion losses. It has recently been claimed [37] that the He^3/Ne^{21} ratio of 3.0 in the chondrite Weldona is due to strong diffusion loss. However, ZÄHRINGER [26] reports $Ne^{22}/Ne^{21} = 1.04$ and thus this meteorite lies close to the correlation line in Fig. 3.

6.2 Radiation Ages

The radiation age T_R of a meteorite is defined as

$$T_R = C^I/P_0^I \qquad (2)$$

where C^I is the concentration of a stable spallation isotope and P_0^I its production rate just prior to the fall of the meteorite. P_0^I can be inferred from the concentration of a suitable radioactive spallation isotope, such as H^3. Several different possible irradiation histories for stone meteorites have been proposed and discussed (cf. EBERHARDT, EUGSTER, and GEISS [43]). The most simple and basic one assumes that the meteorite was completely shielded from cosmic radiation until it was broken out of a larger body and exposed. If the production rate was constant during the whole exposure time, then the radiation age T_R dates this event.

Measurements of tritium in a number of chondrites have shown that the production rate of He^3 is the same in chondrites within approximately $\pm 20\%$ (l. c. [40, 41]). Thus, it is possible to calculate radiation ages of chondrites from He^3 concentrations alone, using an average production rate of 2×10^{-8} cc STP He^3/m.y. The error introduced by this assumption should be less than $\pm 20\%$.

Several authors have also derived radiation ages from Ne^{21} concentrations. However, the neon production rate is less constant than that of He^3 (see 6.1). Radiation ages calculated from Ne^{21} concentrations alone are therefore liable to have large errors. The same holds for radiation ages calculated from Ar^{38}.

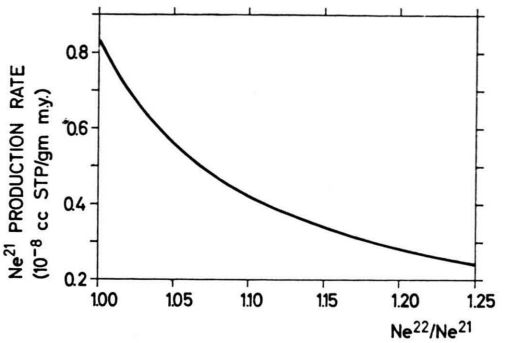

Fig. 5. Ne^{21} spallation production rate as function of $(Ne^{22}/Ne^{21})_{spall}$ ratio. A constant He^3 production rate of 2×10^{-8} cc STP/gm m. y. was assumed.

The correlation discovered between the He^3/Ne^{21} and Ne^{22}/Ne^{21} ratios can now be used for deriving Ne^{21} production rates. In Fig. 5 the Ne^{21} production rate is given as function of the Ne^{22}/Ne^{21}ratio. It has been calculated from Eq. (1), assuming constant He^3 production rate. In this way radiation ages can also be obtained from Ne^{21} concentrations, provided the Ne^{22}/Ne^{21} ratio has been measured with sufficient accuracy.

The radiation ages of the investigated meteorites are given in Table 6. They were calculated by assuming a constant He^3 production rate of 2×10^{-8} cc STP He^3/m.y. The ages obtained are in agreement with the salient features found for the radiation age distributions of the different chondrite classes (GEISS, OESCHGER, and SIGNER [40]); EBERHARDT and GEISS [8]; ANDERS [25]; ZÄHRINGER [26]). A detailed discussion seems therefore unnecessary.

7. Trapped Gases

In the course of this work we have found several new chondrites with large amounts of trapped gases (primordial gases). These are Tysnes Island and Dimmitt, containing "solar type" trapped gases; Mezö-Madaras, Tieschitz and Marion with "planetary type" trapped gases. Also Pseudo-Pultusk is a gas-rich meteorite, in accordance with He and Ne measurements on Pultusk [35]. The rare gas concentrations and isotopic composition in the trapped gas component of these and other meteorites will be discussed elsewhere.

Acknowledgements

The authors are greatly indebted to their collegues who supplied and prepared the meteorite samples used in this investigation: Prof. W. SCHOLLER, Naturhistorisches Museum, Wien; Dr. E. P. HENDERSON, U.S. National Museum, Washington; Prof. C. B. MOORE, Arizona State University, Tempe; Prof. J. ARNOLD, University of California, San Diego; Dr. G. KURAT, Naturhistorisches Museum, Wien; Prof. M. GRÜNENFELDER, ETH, Zürich; Prof. A. DE CASTELLO BRANCO, Serviços Geologicos, Lisboa; Prof. A. TUCEK, Narodni Museum, Praha; Prof. R. E. FOLINSBEE, University of Alberta, Edmonton; Proffs. R. DAVIES and O. SCHAEFFER, BNL, Brookhaven.

We are indebted to Dr. N. GRÖGLER for advice and help in the preparation of the meteorite samples. Our work has benefitted from stimulating discussions with Proffs. E. ANDERS, N. GRÖGLER, and F. G. HOUTERMANS.

We would like to thank Messrs. E. LENGGENHAGER, H. WYNIGER, H. HOFSTETTER, and R. LINIGER for their careful work in constructing the mass spectrometers; Miss A. STROTZ and Messrs. R. GASSER and T. REBER for their assistance in preparing and analyzing the samples; and Miss B. RAMSEIER for the preparation of the manuscript.

This work was supported by the Swiss National Science Foundation grants KAW/A 214, NF 2648, NF 3045, and NF 3468.

Kraftkonstantenberechnung nach einer Methode der nächsten Lösung

A. FADINI *

Lehrstuhl für Technische Mechanik (Prof. SLIBAR) der Technischen Hochschule, Stuttgart

(Z. Naturforschg. **21 a**, 426—430 [1966]; eingegangen am 30. November 1965)

Die Berechnung von Molekülkraftkonstanten aus der Säkulargleichung $|\mathbf{G}\cdot\mathbf{F}-\lambda\mathbf{E}|=0$ führt im allgemeinen auf eine unendliche reelle Lösungsmannigfaltigkeit **F**, wenn nur die inverse Matrix **G** der kinetischen Energie und die Spektralmatrix $\mathbf{L}=\mathrm{Diag}(\lambda_i)$ mit $i=1, 2, \ldots, n$ bekannt sind. Bei einer Reihe von Molekülen können Näherungslösungen $\mathbf{F}_{\text{näh}}$ bestimmt werden, und wir geben ein Verfahren an, durch das aus **F** eine Matrix $\mathbf{F}_{\min}$ als Kraftkonstantenmatrix ausgewählt wird, die der Näherungslösung $\mathbf{F}_{\text{näh}}$ am nächsten liegt. Für dieses sogen. erweiterte inverse Eigenwertproblem der Ordnung $n=2$ wird die Bedingung für die Existenz eines reellen Lösungsbereiches angegeben, die Lösungsmethode als Näherungsverfahren explizit dargestellt und das mathematische Modell der nächsten Lösung geometrisch interpretiert. An den beiden Molekülen BrCN und OCS wird das Verfahren erprobt. Im Falle gleicher Eigenwerte existiert für $n=2$ nur die eine reelle Lösung $\mathbf{F}(\lambda)=\lambda\cdot\mathbf{G}^{-1}$.

1. Die Berechnung von Molekülkraftkonstanten als „ein erweitertes inverses Eigenwertproblem“ [1]

Die klassische Theorie der Molekülkraftkonstanten führt auf die Berechnung der Kraftkonstantenmatrix **F** aus der Säkulargleichung

$$\det(\mathbf{G}\cdot\mathbf{F}-\lambda\mathbf{E})=0\,. \tag{1}$$

Dabei wird die Matrix **G** aus den Gleichgewichtsabständen, den Valenzwinkeln und Atommassen in gegebener Anordnung berechnet. Die Spektralmatrix $\mathbf{L}=\mathrm{Diag}(\lambda_i)$ mit $i=1, 2, \ldots, n$ ergibt sich aus den n Schwingungsfrequenzen des Moleküls, die dem RAMAN- oder den Ultrarotspektren entnommen werden.

Für $\mathbf{F}=\mathbf{F}_{\text{diag}}$ existieren $n!$ reelle und komplexe Lösungen [2]. Bei der Kraftkonstantenrechnung ist jedoch **F** mit

$$\mathbf{F}=\mathbf{F}_{\text{sym}}=(f_{ik})=(f_{ki}) \text{ mit } i, k=1, 2, \ldots, n \tag{2}$$

gesucht und dies führt im allgemeinen auf eine unendliche Lösungsmannigfaltigkeit für **F**. Wegen der Realität der Kraftkonstanten setzen wir die Existenz einer reellen Lösungsmannigfaltigkeit für **F** voraus.

Für eine Reihe von Molekülen ist es durch Hinzunahme zusätzlicher Daten möglich, physikalisch hinreichend genaue Näherungslösungen

$$\mathbf{F}_0=\mathbf{F}_{\text{sym},0}=\mathbf{F}_{\text{näh}} \tag{3}$$

anzugeben (siehe Abschnitt 3). Die beiden physikalischen Aussagen (1) und (3) werden sinnvoll

* Privatanschrift: 74 Tübingen, Breuningstr. 31.

[1] Das hier dargestellte Eigenwertproblem wurde bereits auf der GAMM-Tagung in Wien im April 1965 vorgetragen und das Lösungsverfahren „Quadratsummen-Minimum-Verfahren“ genannt [14]. Die geometrische Interpretation wurde auf dem 8. Europäischen Kongreß für Spektroskopie in Kopenhagen vom 14.—20. August 1965 vorgebracht [15].

[2] J. UHLIG, Z. Angew. Math. Mech. **38**, 284 [1958].